Accepted Manuscript

Synthesis, characterization and antitubercular activities of novel pyrrolyl hydrazones and their Cu-complexes

Shrinivas D. Joshi, Devendra Kumar, Sheshagiri R. Dixit, Nageshwar Tigadi, Uttam A. More, Christian Lherbet, Tejraj M. Aminabhavi, Kap Seung Yang

PII: S0223-5234(16)30413-5

DOI: 10.1016/j.ejmech.2016.05.025

Reference: EJMECH 8617

To appear in: *European Journal of Medicinal Chemistry*

Received Date: 23 January 2016

Revised Date: 7 May 2016

Accepted Date: 9 May 2016

Please cite this article as: S.D. Joshi, D. Kumar, S.R. Dixit, N. Tigadi, U.A. More, C. Lherbet, T.M. Aminabhavi, K.S. Yang, Synthesis, characterization and antitubercular activities of novel pyrrolyl hydrazones and their Cu-complexes, *European Journal of Medicinal Chemistry* (2016), doi: 10.1016/j.ejmech.2016.05.025.

GRAPHICAL ABSTRACT

Synthesis, characterization and antitubercular activities of novel pyrrolyl hydrazones and their Cu-complexes

Shrinivas D. Joshi, Devendra Kumar, Sheshagiri R. Dixit, Nageshwar Tigadi, Uttam A. More, Christian Lherbet, Tejraj M. Aminabhavi, Kap Seung Yang

Synthetic route for the synthesis of biologically active metal complexes as enoyl ACP reductase inhibitors

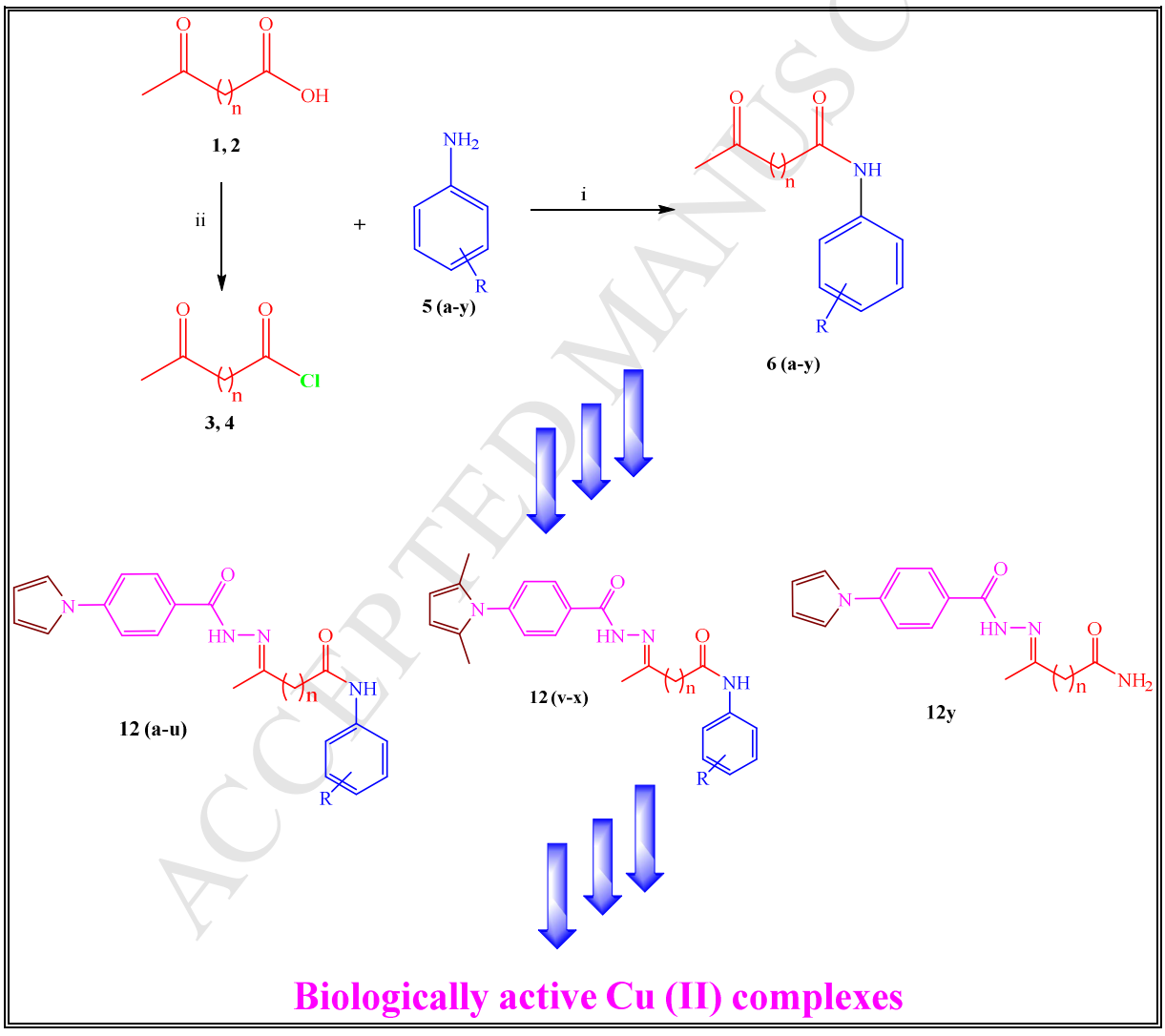

Synthesis, characterization and antitubercular activities of novel pyrrolyl hydrazones and their Cu-complexes

Shrinivas D. Joshi*[a], Devendra Kumar[a], Sheshagiri R. Dixit[a], Nageshwar Tigadi[a], Uttam A. More[a], Christian Lherbet[b,c], Tejraj M. Aminabhavi[a], Kap Seung Yang[d]

[a]*Novel Drug Design and Discovery Laboratory, Department of Pharmaceutical Chemistry, S.E.T's College of Pharmacy, Sangolli Rayanna Nagar, Dharwad-580 002, India.*

[b]*Universite de Toulouse, UPS, Laboratoire de Synthese et Physico-chimie de Molecules d'Interet Biologique, LSPCMIB, 118 Roote de Narbonne, F-31062, Toulouse Cedex 9, France.*

[c]*ITAV-USR3505, Université de Toulouse, CNRS, UPS, F-31106 Toulouse, France.*

[d]*Department of Polymer and Fiber System Engineering, Chonnam National University, 300 Yongbong-Dong, Bukgu, Gwangju, 500 757, Korea*.

Corresponding Author

Shrinivas D. Joshi, Novel Drug Design and Discovery Laboratory, Department of Pharmaceutical Chemistry, S.E.T's College of Pharmacy, Sangolli Rayanna Nagar, Dharwad-580 002, India.
E-mail: shrinivasdj@rediffmail.com.
Tel.: +91 9986151953; Fax; +91 836 2467190

Abstract

Novel pyrrolyl hydrazones and their copper complexes have been synthesized and characterized using analytical and spectral techniques to show the tetrahedral geometry for Cu(II) complexes. Biological activities of hydrazones have been assessed to understand the role of metal ion on their biological activity and the effect of pyrrolyl hydrazones. *In vitro* antitubercular activity against *Mycobacterium tuberculosis* of the metal complexes (**13b** and **13r)** exhibited the highest antitubercular activity that are quite close to rifampicin (0.4 µg/mL), giving a MIC of 0.8 µg/mL. All other compounds showed good activity with the MIC values ranging from 1.6-100 µg/mL. A comparative study of inhibition values of the ligands and their complexes showed higher antimicrobial activity of the complexes than the ligands. Some compounds have a good activity against InhA and in particular, compounds **12r, 13b** and **13r** exhibited more than 60% binding with the enzyme even at 5 µM (exhibited good IC50 upto 2.4 µM). Most of the active molecules have a very less cytotoxicity against the human lung cancer cell-line A549. The docking and 3D-QSAR studies have been carried out to provide some insights into the mechanism of action for this class of compounds.

Keywords: Surflex docking, Pyrrolyl Schiff bases, Pyrrolyl Cu-complexes, Anti-tubercular activity, Cytotoxicity activity, Enzyme inhibition studies.

1. Introduction

Tuberculosis (TB) is the leading airborne contagious disease caused by *Mycobacterium tuberculosis* (MTB) and is the second leading cause of death worldwide [1]. TB is known to be one of the major causes of death in HIV patients. As per World Health Organization (WHO) 2012 global report on TB, an estimated 3.7% (range 2.1-5.2%) of new cases and 20% (range 13-26%) of the previously treated cases show multidrug-resistant TB (MDR-TB) features. In Eastern Europe and central Asia, nearly 9-32% of new cases and more than 50% of the previously treated patients acquired MDR-TB [2]. Global increase in drug resistance, mainly MDR-TB, reflects at least in part, improper use of anti-TB drugs during the treatment course of TB patients with drug susceptible strains [3]. Additional factors such as sex, age, HIV infection and socio-economic factors have also shown to be responsible for increased prevalence of MDR-TB [4]. Nearly 50% of global MDR-TB cases have been reported in China and India [5].

Currently, TB treatment using DOTS (directly observed therapy short-course) requires a combination of three to four drugs, which includes isoniazid, pyrazinamide, rifampin, and ethambutol for over a period of 6-12 months. The extended treatment schedule for TB is due to the presence of non-replicating persistent MTB phenotype and therefore, novel drugs are urgently required for the treatment of this deadly disease.

Isoniazid (INH), a frontline antitubercular agent, is a pro-drug that requires activation to form active metabolite (INH-NAD adduct), which exerts its lethal action on intracellular target [6, 7]. The INH-NAD adduct inhibits mycolic acid biosynthesis in MTB by affecting InhA, a 2-*trans*-enoyl-acyl carrier protein reductase enzyme of the type II fatty acid synthesis (FAS-II) system, which catalyses the last step of fatty acid elongation cycle [8]. Among them, fatty acid biosynthesis-I (*FabI*) constitutes a single isoform in major pathogens such as *Staphylococcus aureus* [9], *Escherichia coli* [10], and MTB [11]. The clinical success of

InhA inhibitor isoniazid [12] and numerous reports of *FabI* inhibitors [13] involving diazaborines [14], 4-pyridones [15], naphthyridinones [16], triclosan and its analogues [17, 18] have validated this target as one of the most attractive of the FAS-II pathways. This enzyme is recognized and validated as an important drug target in MTB, since its homolog in human is absent.

Several azole compounds containing imidazole, pyrrole, toluidine or methanamine group were tested for anti-TB activity against drug resistant and intramacrophagic mycobacteria [19]. Amongst these compounds, pyrrole derivative BM212 appeared to be particularly potent due to its selective antimycobacterial properties [20]. Recently, spontaneous mutants resistant to BM212 and SQ109, compounds with anti-TB activities, were shown to contain mutations mapping to *mmpL3* (for mycobacterium large membrane protein) [21]. The *mmpL3* was found to be essential in mycobacteria and conditional depletion of *mmpL3* in *Mycobacterium smegmatis* resulted in a loss of cell wall mycolylation [22].

Realizing the widespread application of transition metal complexes in living systems [23-25] and due to their favorable biological activity [26], the complexes of tetradentate Schiff base ligands with transition metals (manganese, copper and nickel) have been shown to exhibit antibacterial, antifungal and cytotoxicity activities [27-29]. In our earlier studies, we have developed a new series of compounds that have shown promising antimycobacterial activities [30, 31]. However, keeping in view of the biological and medicinal properties of pyrroles and the potentiality of transition metal chemistry, it was felt necessary to design metal complexes with organic ligands such as pyrrolyl hydrazone having biological activity that could help to treat against the resistant bacteria species. As per Fig. 1, some marketed drugs that were considered in the synthesis of new derivatives following the *Paal-Knorr* pyrrole synthesis, wherein we have designed novel concepts to describe the framework to understand their mechanisms by combining molecular docking and other parameters for their structural

characteristics that affect the binding of pyrrolyl hydrazones and copper complexes with enoyl ACP reductase receptor. Molecular docking studies have been used to correlate *in silico* results with *in vitro* analysis to find ENR as a potential target for these derivatives.

2. Molecular modeling/docking studies

The 3D structures were generated using SYBYL package (Tripos Associates, St. Louis, MO, USA) [32]. By using standard bond lengths and bond angles, the geometry optimization was carried out with the help of standard Tripos Force Field [33] with a distance dependent-dielectric function, energy gradient of 0.001 kcal/mol and Gasteiger-Huckel as the electrostatics. Conformational analysis of all the ligands was performed using the repeated molecular dynamics-based simulated annealing approach as implemented in Sybyl-X 2.0. All the conformations were minimized with Gasteiger-Huckel charges.

2.1. Data set and structures

The *in vitro* antitubercular activity (expressed as MIC) was converted into pMIC (log MIC) values, which were used to construct 3D-QSAR models. Antitubercular activity results of the synthesized compounds are summarized in Table 1. The 3D-QSAR models were generated using a training set of 19 molecules, and predictive power of the resulting models was evaluated using a test set of six molecules. Test compounds were selected randomly by diversity method such that the data set included diverse structures and a wide range of activity.

2.2. Alignment rule

A common substructure-based alignment was adopted, wherein molecules were aligned to the template molecule on a common backbone. For database alignment of the inhibitors, the structure of compound **12b** was used as a templet.

2.3. CoMFA and CoMSIA settings

In order to understand the contributions of electrostatic and steric fields in the binding affinity and potency of pyrrole scaffold, as well as to build the predictive 3D-QSAR models, the CoMFA studies were performed on the ligands based on molecular alignment. The contributions of steric and electrostatic fields were calculated using the Lennard-Jones and

Coulombic potentials, respectively [34]. The aligned training set of molecules was then placed in a 3D grid box to include the entire set. The CoMFA steric and electrostatic fields were generated at each grid point with Tripos force field using sp^3 carbon atom with +1 charge.

The CoMSIA was used in which similarity indices (steric, electrostatic, hydrophobic and H-bond donor and H-bond acceptors) were calculated at different points on a regularly spaced grid for pre-aligned molecules with a radius of 1.0 Å and a default value of 0.3 as the attenuation factor (α), a grid spacing of 2.0 Å in x, y, and z directions used for both CoMFA and CoMSIA. The q^2 resulted in an optimum number of components and the lowest standard error of prediction.

2.4. Partial least squares (PLS)

PLS analysis provides a correlation between anti-TB activity of the compounds with the predictive values of CoMFA and CoMSIA containing a magnitude of steric, electrostatic, hydrophobic potentials, H-bond donor, and acceptor. This regression method was used to analyze the training set by correlating dependent variable values (anti-TB activity) with variations in their independent variables (CoMFA/CoMSIA interaction fields). All the latent variable path models in PLS consist of three sets of relationships: (a) the inner model, which specifies the relationship between latent variables (LVs), (b) the outer model, which specifies the relationship between LVs and their association observed or manifest variables (MVs), and (c) the weight relations upon which the case values for LVs can be estimated. Without loss of generality, it can be assumed that LVs and MVs are scaled to zero means and unit variance such that location parameter (*i.e.*, constant parameter terms) can be eliminated [35].

2.5. Predictive ability of CoMFA and CoMSIA models (r^2_{pred})

The value of r^2 is a measure of % of data that can be satisfactorily explained by the regression analysis [36]. Predictive ability of each analysis was determined from the test set molecules

that were not included in the training set. These molecules were aligned and their activities were predicted by each PLS analysis.

By PLS analysis, r^2 predicted for CoMFA and CoMSIA were found to be 0.86 and 0.69, respectively. Cross validated and non-cross validated statistical parameters of CoMFA and CoMSIA models are summarized in Table 2.

3. RESULTS AND DISCUSSION

3.1. Chemistry

Studies were undertaken to synthesize novel pyrrole ring bearing hydrazone derivatives and their copper complexes to investigate their anti-TB effects. Compounds **6a-y** were synthesized as per Scheme 1. Various carboxamides were synthesized by reacting the commercially available acids viz., pyruvic acid **(1)** / lavulanic acid **(2)** in the presence of thionyl chloride or HBTU [(*N*,*N*,*N*′,*N*′-tetramethyl-*O*-(1*H*-benzotriazol-1-yl)uraniumhexa fluorophosphate] /DIEA (*N*,*N*-diisopropylethylamine). Pyrrole synthesis is achieved via *Paal-Knorr* mechanism by the condensation of 2,5-dimethoxytetrahydrofuran or 1,4-diketone (2,5-hexanedione) and ethyl 4-amino benzoate **(7)** in the presence of dry acetic acid to get 4-(1*H*-pyrrol-1-yl)benzoate **(8)** or 4-(2,5-dimethyl-1*H*-pyrrol-1-yl)benzoate **(9)** in good yield**.** Thus obtained esters were converted to their corresponding hydrazides **(10, 11)** by hydrazinolysis using hydrazine hydrate (Scheme 2). The NH_2 in hydrazides **(10, 11)** is more nucleophilic than NH, which reacts preferentially with the more reactive carbonyl group **(6a-y)**, leading to the formation of hydrazone derivative **(12a-y)** (Scheme 3) as the major products, especially if the reaction is carried out in the presence of a catalytic amount of acetic acid or TFAA upon heating or without heating.

The structures of hydrazones **(12a-y)** were established by spectral analysis. The compound **12r** showed characteristic absorption bands at 1701 cm^{-1} and 1687 cm^{-1} for carbonyl groups and the absence of NH_2 stretching band around 3335 cm^{-1}. A sharp peak at 1577 cm^{-1}

indicates the presence of C=N group. The ^{1}H NMR showed two singlets at 9.88 and 10.54 δ ppm corresponding to two -NH protons. A singlet at δ 1.98 ppm, which, was accounted for three protons of methyl group and a multiplet at δ 2.51-2.56 ppm representing the four protons of pentamide. All other 12 protons of aromatic rings resonated in the expected region between δ 6.29-8.23 ppm. The number of protons calculated from the integration curves and those obtained from the values of the expected CHN analyses agree with each other.

3.2. Synthesis and characterization of copper complexes

The synthesis of copper complexes was carried out as per Scheme 4. Hydrazones **(12a-y)** were reacted with copper acetate in a refluxing ethanol medium to furnish the targeted copper complexes **(13a-y)**, which were readily soluble in DMSO and DMF solvents. They are non-hygroscopic and stable in both solid and solution phases. The elemental analyses data for Cu (II) complexes are in good agreement with their molecular formulae and all metal complexes are green in color.

3.3. FTIR spectra

FTIR spectra of the metal complexes are compared with that of the ligand itself to find the coordination sites involved in the bond formation. There are some guide peaks in the spectrum of the ligand, which enabled us to understand this aspect. These peaks change either in their positions and/or their intensities upon chelation, but some peaks disappeared after chelation.

The carbonyl stretching bands found in the region of 1603-1714 cm^{-1} **(12a-y),** which have disappeared, indicating the involvement of carbonyl group in bond formation with metal, while two -C=N peaks are observed in FTIR spectrum of the metal complex. From these observations, it can be concluded that two carbonyl groups of the ligand have undergone mesomerism, since the mesomeric form containing -C=N-N-O^{-} type of arrangement might be involved in the bond formation with the central metal. Further, this type of mesomerism was

proved by the appearance of two -C=N- stretching bands in the region of 1690-1579 cm^{-1} (medium band). From the FTIR spectra, it was found that hydrazide nitrogen might have been involved in coordinate bond formation with the central metal ion **(13a-y)**.

3.4. UV-Visible Spectroscopy

UV (ultraviolet)-visible spectroscopy was used at >300 nm to analyze the geometry of metal complexes, which confirmed tetrahedral geometry.

3.5. Thermogravimetric analysis

Water of hydration is related with the central metal ion complex formation around the coordination sphere, which generally takes place around the temperature range of 50-140°C, indicating no loss of any fragment around the water molecule. This further confirmes that there is no water molecule attached outside the coordination sphere. The coordinated water molecules directly bonded to metal ion are generally knocked off at higher temperature of 150-250°C [35-37]. However, mass spectrometry suggests that complexes may not contain water molecule either inside or outside the coordination sphere, which further confirms the results of TGA.

Metal complexes decompose at 195-285°C in two steps via the formation of unstable intermediates ending at 490-750°C (oxides formation). The % metal complexes were calculated from the % residual metal oxide formed in the final step, and these are in good agreement with the results obtained by MacDonald wet combustion method [40]. TGA data of copper complexes are summarized in Table 3. On the basis of the above observations, following general scheme for thermal decomposition can be proposed for metal complexes in the ratio of 1:2 (M:L)

$$[ML_2]CH_3OH \xrightarrow[55 - 70^oC]{\text{Solvent removal}} [ML_2]$$

$$[ML_2] \xrightarrow[230 - 320\ ^oC]{\text{Decomposition}} \text{Intermediate}$$

$$\text{Intermediate} \xrightarrow[680 - 1001\ ^oC]{\text{Final decomposition}} \text{metal oxide}$$

3.6. Mass spectrometry

Mass spectroscopy was used to determine the ratio of ligands involved in the complex formation with the central metal ion as well as to estimate the mole reactants used in the synthesis. It also gives appropriate information about the involvement of water or chlorine molecule during the complexation step. In this study, neither water nor chlorine was involved in the formation of the coordination sphere. Molecular ion peak for ligand (**12r**) is observed at 392 *m/z*, whereas its copper complex **13r** shows molecular ion peak at 844 *m/z*, which confirms the molecular weight of **12r** and **13r**.

3.7. Cyclic voltammetry

Cyclic voltammetry of the complexes were performed on 0.025M solutions in DMSO solvent containing 0.2M $[NBu_4][ClO_4]$ in acetonitrile as the supporting electrolyte in the range of +1 to -0.4 V. All solutions were purged with nitrogen gas for 5 min before measurement and working electrode was polished before each experiment with 0.5 µ particle size α-alumina slurry. The procedure was performed at room temperature and nitrogen atmosphere was maintained over the solution during measurements. In the positive range of +1 to 0 V the oxidation of Cu(III) to Cu(II) was observed.

3.8. Stability of complexes in solution

The stability of complexes in aqueous solution was studied by observing UV-VIS spectra. The compounds were prepared in DMSO solvent and for experiments freshly diluted in phosphate buffer system. UV-VIS spectra and molar conductivities were measured at

different time intervals. It can be seen from the results show that there are no change in absorption bands, indicating that these complexes are quite stable in phosphate buffer.

3.9. Molecular modeling

In order to investigate detailed intermolecular interactions between the ligand and the target protein, a program Surflex-Dock was used. The 3D structure information on target protein was taken from PDB entry 2AQI [41] (Crystal structure of isoniazid-resistant I47T enoyl ACP (CoA) reductase mutant enzyme from *MTB* in complex with NADH). Processing of the protein included the removal of ligand and solvent molecules as well as addition of essential hydrogen atoms. All 50 compounds were docked into active site of the enzyme and predicted binding energies of the compounds are listed in Tables 4 and 5.

As depicted in Fig. 2, fluorine atom attached to aromatic ring of compound **12r** makes two H-bond interaction (F-----H-PHE41, ASP42) i.e., hydrogen of amide linkage attached to 4-fluoro phenyl ring makes one bonding interaction with SER94 (NH-CO-----O-SER94) and oxygen of another amide linkage attached to bridging phenyl makes one H-bonding interaction (CONH------H-THR196). As depicted in Fig. 3 (A and B), the hydrogen of hydrazide of compound **13b** makes bonding interaction with amino acid residue (NH----H-GLY96).

It was found that hydrophobic region of mutant ENR enzyme overlap with the hydrophobic region of copper complex (Fig 3B) and due to such type of overlapping as well as involvement of different forces such as van der Waals, and π-π interaction along with H-bonding are strong base for such interaction between copper complex and mutant ENR enzyme.

3.10. CoMFA and CoMSIA models

3.10.1. Contour maps

Steric and Electrostatic field. In 3D-QSAR analysis, a very less difference between the actual pMIC and predicted pMIC was observed (Table 6). From the 3D-CoMFA analysis, it can be confirmed that if the steric bulk is increased on pyrrole ring, biological activity of the compound will be diminished (Fig 4A) as was also supported by CoMSIA analysis (Fig. 5A). In CoMSIA, the blue counter map on pyrrole confirms that this is the sterically disfavored region. This is one of the causes of decrease in biological activity of some of the derivatives having the methyl group on their 2^{nd} and 5^{th} positions with ligands such as **12v** (exceptional), **12w** and **12x** that suffer from an increase in MIC values up to 12.50, 100 and 25 µg/ml, respectively. In docking analysis, it was found that all these methyl containing pyrrole ligands have less binding affinity with the mutant ENR enzyme. The ligands **12v**, **12w** and **12x** have the binding scores of 4.52, 4.47 and 3.97, respectively along with a slightly high crash score. Benzene ring that is directly attached to the pyrrole contains a big section of blue contour map, due to the bulky group of unfavorable contour. Blue contour map on anilide benzene ring reveals that substitution on this ring is less bulky, but cyan contour map in CoMFA and CoMSIA over this ring is a clear indication of the electronegative substitution (Fig. 4B and Fig. 5B).

Hydrogen-bond-acceptor field. In Fig. 5C, it can be observed that in the highly active template molecule **12b**, the green contour in the region of hydrazone bridge favors its activity.

Hydrogen-bond-donor field. In Fig. 5D, pink contour on NH of anilide and also on hydrazone bridge of molecule **12b** favor the activity.

Hydrophobicity field. According to CoMSIA model, as shown in Fig. 5E, hydrophobicity is favored near the anilide ring (purple contour).

3.11. Antimycobacterial studies and InhA enzyme inhibition studies

The MIC values were determined for hydrazones **(12a-y)** and their copper complexes **(13a-y)** against *M. tuberculosis* strain H37Rv using the Microplate Alamar Blue assay (MABA) method using ethambutol and rifampicin as the standard drugs. The tested compounds showed activities against mycobacteria with the MIC values ranging from 0.8 to 100 µg/mL (Table 1). In most of the cases, higher activity was exhibited by the copper complexes than the ligands. Compounds **13b, 13h, 13o** and **13r** inhibited mycobacterial growth very effectively compared to other tested compounds with the MIC values ranging from 0.8 and 1.6 µg/mL.

By considering *in vitro* antimycobacterial studies, we have selected ten compounds for *in vitro* enzyme inhibition activity against InhA from *M. tuberculosis* at 50 µM (and/or at 5 µM) by utilizing the commonly used approach. [42] (Table 7). Triclosan was used as reference and showed a complete inhibition of InhA enzyme at 50 µM.

Ligand **12r** having fluorine at the 4th position exhibited 100% binding with the enzyme with IC_{50} at 7.7 µM. The corresponding copper complex **(13r)** showed the same activity profile with IC_{50} at 2.4 µM. This increase in biological activity is due to high electro-negativity and small size of the substituent on the 4th position of anilide ring. The molecule **12b** also showed remarkable value of 35% binding and its copper complex **(13b)** had extraordinary binding affinity with the enzyme viz., 100% at 50 µM (IC_{50} = 2.4 µM). The molecule **12o** and its copper complex **13o** also passes the notable binding affinity with enzyme.

3.12. Cytotoxicity

Among the 10 compounds utilized for enzyme assay, seven most promising compounds were taken forward for cytotoxicity study against the human lung cancer cell-line A549 (Table 8). It was concluded from cytotoxic activity that the most active ligand molecules are very much safe towards human lung cell-line. Compounds **12b**, **12o** and **12r** showed IC_{50} that are almost

overlapping with the standard compound (INH). The cytotoxic activity of copper complexes is in the acceptable range of 281-305 µM concentration.

3.13. Structure-activity relationship

From the results of CoMFA, CoMSIA, and docking analysis, it was concluded that all those molecules having electronegative substitution on the 4th position of anilide ring might have favored the biological activity, as in case of ligands containing 4-F, 4-Br or 4-Cl that have shown the best anti-TB activities along with a high binding interaction with the mutant ENR enzyme. Compounds **12b** and **12r** (MIC=3.12 µg/mL) exhibited the best docking pose with the mutant ENR enzyme having total docking scores of 7.96 and 8.01, respectively. The copper complexes of these ligands have shown even better scores with the mutant ENR enzyme. Copper complexes **13b** and **13r** (MIC 0.8 µg/mL) have shown the total docking scores of 11.96 and 12.71 against the mutant ENR. Ligands **12h, 12k** and **12o** having 4-F, 4-Br and 4-Cl substitutions have shown the MIC values of 6.25, 6.25 and 3.12 µg/mL respectively. All these observation suggest that copper complexes of these ligands have a much better biological activity; **13h, 13k** and **13o** have the MIC value of 1.60, 3.12 and 1.60 µg/ml, respectively. Requirement of different substitution pattern on the ligand molecule to get the desirable biological activity are depicted in Fig 6.

4. EXPERIMENTAL SECTION

Kinetic studies were performed on a Cary Bio 100. All chemicals were obtained from Aldrich and used without further purification. Melting points were determined using Shital-digital programmable apparatus and are uncorrected. FTIR spectra in KBr pellets were recorded on a Bruker FTIR spectrophotometer. The ^{1}H and ^{13}C NMR spectra were recorded on a Bruker AVANCE II at 400 and 100/75 MHz, respectively; chemical shifts are expressed in parts per million (ppm) relative to TMS. The abbreviations used to describe the peak patterns are: (b) broad, (s) singlet, (d) doublet, (t) triplet, (q) quartet, and (m) multiplet. Since copper (II) complexes are paramagnetic in nature hence, their NMR spectra could not be obtained.

Mass spectra (MS) were recorded on a JEOL GCMATE II GC-Mass spectrometer and Schimadzu QP 20105 GC-Mass spectrometer. Elemental analysis data (performed on Leco Tru Spec CHNS Analyzer) for C, H, and N fall within 0.4% of the theoretical data. Thin-layer chromatography (TLC) was performed on pre-coated TLC sheets of silica gel 60 F254 (Merck, Darmstadt, Germany) visualized by long- and short-wavelength UV lamps. Chromatographic purifications were done on Merck aluminum oxide (70-230 mesh) and Merck silica gel (70-230 mesh). UV-spectra were recorded on a Shimadzu spectrophotometer. Electrochemical studies were carried out on a CHI-1103a electrochemical Analyzer (CH Instruments Ltd. Co., USA, version 12.01) electrode system involving a GCE (3 mm diameter) as the working electrode, a platinum wire as a counter electrode and an Ag/AgCl as reference electrode, standardized for the redox couple ferricinium/ferrocene ($E_{1/2}$=+0.400 V, ΔE_p=60 mV).

4.1. General procedure for the synthesis of 3-oxo-N-substituted phenylpentamides or 2-oxo-N- substituted phenylpropamides **6(a-y)**

Compounds **[6(a-f), 6(k-p), 6v, 6w, 6y]** were prepared by heating a mixture of levulinic acid **1** (1 mol) or pyruvic acid **2** (1 mol) and thionyl chloride (2.5 mol) at 70 ºC for 30 min. The

reaction was monitored using TLC. After cooling the reaction mixture, excess of thionyl chloride was distilled off to get compounds 2-oxopropanoyl chloride **3** and 4-oxopentanoyl chloride **4**. To this crude product, a solution of substituted anilines in diethyl ether was added and continued heating for another 30 min. and the reaction was monitored using TLC. After cooling to ambient temperature, the separated solid was filtered, washed with diethyl ether and acetonitrile, and purified by column chromatography on silica gel with a mixture of chloroform: ethyl acetate (6:4).

For preparation of compounds [**6(g-j), 6(q-t), 6u, 6x**], compounds **1** and **2** (0.0019 mol) and different anilines (0.0018 mol) were dissolved in dry DMF solvent (58 mL). HBTU (0.87g, 0.0023 mol) and DIEA (0.93 mL, 0.0053 mol) were added and stirred for 42-48 h at 23 ^{o}C. The reaction was monitored using TLC, and after completion of the reaction, mixture was poured onto distilled water. The resulting mixture was extracted with a mixture of ethylacetate:methanol (9:1). The organic layer was dried over anhydrous sodium sulphate. The residue left out after concentrating the organic layer in vacuum was purified by column chromatography on silica gel with a mixture of chloroform: ethyl acetate (6:4).

*4.2.1. Synthesis of 4-(1H-pyrrol-1-yl)benzoic acid hydrazide **10***

Ethyl 4-(1*H*-pyrrol-1-yl)benzoate **8** (15 mmol) was refluxed with hydrazine hydrate (10 mL) in absolute ethanol (10 mL) for 3 h. The reaction mixture was cooled and the crystalline mass obtained was further recrystallized from ethanol [45].

*4.2.2. Synthesis of 4-(2,5-dimethylpyrrol-1-yl)benzoic acid hydrazide **11***

Compound **11** was synthesized by refluxing a mixture of ethyl 4-(2,5-dimethylpyrrol-1-yl)benzoate **9** (3.64 g, 15 mmol) with hydrazine hydrate (10 mL) in absolute ethanol (10 mL) for 3 h (monitored by TLC). The cooled mixture was poured gradually onto the crushed ice with stirring. The mixture was allowed to stand, solid separated, filtered, and washed

thoroughly with cold water, then dried and recrystallized from ethanol (yield 80%). mp 170-172^{0}C [45].

*4.2.General procedure for synthesis of pyrrolyl hydrazones **(12a-y)***

An ethanolic solution of *N*-substituted phenylalkylamides **6(a-y)** (0.005 mol) was added to a hot ethanolic solution of 4-(1*H*-pyrrol-1-yl)benzoic acid hydrazide **10** (0.005 mol) or 4-(2,5-dimethylpyrrol-1-yl)benzoic acid hydrazide **11** (0.005 mol) in the presence of catalytic amount of acetic acid. The mixture was heated under reflux for 72-78 h and cooled to ambient temperature. The crude product was filtered, washed with ethanol, dried and purified using column chromatography on silica gel with a mixture of chloroform:ethyl acetate (6:4) to afford the final compounds **12(a-y)**.

*4.3.1. N-(3-Bromophenyl)-2-{2-[4-(1H-pyrrol-1-yl)benzoyl]hydrazinylidene}propanamide **(12a)***.

(Yield 68%). mp 230-232 °C; FTIR (KBr) cm^{-1}: 3255 (2° amine), 2922 (Ar-H), 1693, 1666 (C=O), 1585 (C=N); ^{1}H NMR (400 MHz, DMSO) δ ppm: 2.24 (s, 3H, -CH_3), 6.30 (t, 2H, pyrrole-C_3, C_4-H), 7.18-7.36 (m, 5H, pyrrole-C_2, C_5-H and bromophenyl-C_4, C_5, C_6-H), 7.64 (t, 3H, bridging phenyl-C_2, C_6 and bromophenyl-C_2-H), 8.01 (d, 2H, bridging phenyl-C_3, C_5-H), 10.39 (s, 1H, hydrazinylidene-NH), 11.07 (s, 1H, propanamide-NH); ^{13}C NMR (75 MHz, DMSO) δ ppm: 11.5, 111.1, 118.3, 118.4, 118.6, 121.5, 122.2, 126, 129.1, 130, 130.1, 139.7, 142.6, 162.5; MS (ESI): m/z found 425.00, 426.14 [M^+, M^+ (1:1)]; calcd. 425.28. Anal. Calcd. For $C_{20}H_{17}N_4O_2Br$: C, 56.48; H, 4.03; N, 13.17. Found: C, 56.52; H, 4.00; N, 13.10; UV-Visible λ_{max}: 320 nm.

*4.3.2. N-(4-Bromophenyl)-2-{2-[4-(1H-pyrrol-1-yl)benzoyl]hydrazinylidene}propanamide **(12b)***

Yield 72%; mp 240-242°C; FTIR (KBr) cm^{-1}: 3247 (2° amine), 3102, (Ar-H), 1663, 1603 (C=O), 1591 (C=N); ^{1}H NMR (400 MHz, DMSO) δ ppm: 2.28 (s, 3H, -CH_3), 6.45 (t, 2H,

pyrrole-C_3, C_4-H), 7.21 (t, 2H, pyrrole-C_2, C_5-H), 7.49 (t, 2H, bromophenyl-C_3, C_5-H), 7.55-7.58 (m, 4H, bromophenyl-C_2, C_6-H and bridging phenyl-C_2, C_6-H), 7.96-7.98 (dd, 2H, bridging phenyl-C_3, C_5-H), 9.0 (s, 1H, hydrazinylidene-NH), 10.09 (s, 1H, propanamide-NH); ^{13}C NMR (75 MHz, DMSO) δ ppm: 11.5, 118.3, 118.4, 121.5, 126, 129.1, 130.1, 139.7, 142.6, 162.5; MS (ESI): m/z found 425.26, 427.14 [M^+, M^{+2} (1:1)]; calcd. 425.28. Anal. Calcd. For $C_{20}H_{17}N_4O_2Br$: C, 56.48; H, 4.03; N, 13.17. Found: C, 55.98; H, 4.00; N, 13.15; UV-Visible λ_{max}: 325 nm.

4.3.3. N-(2,6-Dichlorophenyl)-2-{2-[4-(1H-pyrrol-1-yl)benzoyl]hydrazinylidene} propanamide ***(12c)***

Yield 57%; mp 211-213°C; FTIR (KBr) cm^{-1}: 3287 (2° amine), 2923 (Ar-H), 1670, 1604 (C=O) 1579 (C=N); ^{1}H NMR (400 MHz, DMSO) δ ppm: 1.98 (s, 3H, propanamide-H), 6.29 (t, 2H, pyrrole C_3, C_4-H) 7.39 (t, 3H, pyrrole-C_2, C_5-H and chlorophenyl-C_4-H), 7.62 (dd, 2H, chlorophenyl-C_3, C_5-H), 7.94 (dd, 2H, bridging phenyl-C_2, C_6-H), 8.23 (s, 2H, bridging phenyl-C_3, C_5-H), 9.80 (s, 1H, hydrazinylidene-NH), 11.01 (s, 1H, propanamide-NH); ^{13}C NMR (75 MHz, DMSO) δ ppm: 11.2, 111.5, 118.4, 118.7, 118.8, 121.2, 121.7, 126.4, 129.7, 130.8, 130.4, 139.1, 142.4, 162.8; MS (ESI): m/z found found 414.41, 416.24, 418.56 [M^+, M^{+2}, M^{+4} (9:6:1)]; calcd. 414.07. Anal. Calcd. For $C_{20}H_{16}N_4O_2Cl_2$: C, 57.37; H, 3.84; N, 13.47. Found: C, 57.84; H, 3.88; N, 13.49; UV-Visible λ_{max}: 267 nm.

4.3.4. N-(3,5-Dichlorophenyl)-2-{2-[4-(1H-pyrrol-1-yl)benzoyl]hydrazinylidene} propanamide ***(12d)***

Yield 62%; mp 183-185°C; FTIR (KBr) cm^{-1}: 3235 (2° amine), 2904 (Ar-H), 1701, 1684 (C=O), 1599 (C=N); ^{1}H NMR (400 MHz, DMSO) δ ppm: 2.53 (m, 3H, propanamide-H), 6.31 (t, 2H, pyrrole C_3, C_4-H) 7.41 (t, 3H, pyrrole-C_2, C_5-H and chlorophenyl-C_4-H), 7.68 (d, 2H, chlorophenyl-C_2, C_6-H), 7.98 (d, 2H, bridging phenyl-C_2, C_6-H), 8.20 (s, 2H, bridging phenyl-C_3, C_5-H), 9.80 (s, 1H, hydrazinylidene-NH), 11.01 (s, 1H, propanamide-NH); ^{13}C

NMR (75 MHz, DMSO) δ ppm: 11.5, 111.4, 118.2, 118.6, 118.7, 121.7, 121.1, 126.4, 129.2, 130.4, 130.7, 139.2, 142.4, 162.8; MS (ESI): m/z found 414.42 [M^+]; calcd. 414.07. Anal. Calcd. For $C_{20}H_{16}N_4O_2Cl_2$: C, 57.70; H, 3.86; N, 13.48.Found: C, 57.84; H, 3.88; N, 13.49; UV-Visible λ_{max}: 314 nm.

4.3.5. N'-(1-(4-Methoxyphenylcarbamoyl)ethylidene)-4-(1H-pyrrol-1-yl)benzohydrazide

(12e)

Yield 80%; mp 108-112 °C; FTIR (KBr) cm^{-1}: 3210 (2° amine), 2930 (Ar-H), 1680, 1653 (C=O), 1588 (C=N); ^{1}H NMR (400 MHz, DMSO) δ ppm: 1.19 (s, 3H, -CH_3), 3.63 (s, 3H, -OCH_3), 6.39 (t, 2H, pyrrole-C_3, C_4-H), 7.23 (m, 4H, pyrrole C_2, C_5-H and methoxyphenyl-C_3, C_5-H), 7.60 (d, 2H, methoxyphenyl-C_2, C_6-H), 7.73-7.76 (m, 2H, bridging phenyl C_2, C_6-H), 7.80-7.89 (m, 2H, bridging phenyl C_3, C_5-H), 9.12 (s, 1H, hydrazinylidene-NH), 10.00 (s, 1H, propanamide-NH); ^{13}C NMR (75 MHz, DMSO) δ ppm: 11.2, 50.1, 111.3, 118.6, 118.1, 118.5, 121.6, 121.1, 126.3, 129, 130.6, 130.4, 139, 142.3, 153, 156, 162.5; MS (ESI): m/z found 376.86 [M^+]; calcd. 376.15. Anal. Calcd. For $C_{21}H_{20}N_4O_3$: C, 67.01; H, 5.36; N, 14.88. Found: C, 67.10; H, 5.33; N, 14.86; UV-Visible λ_{max}: 283 nm.

4.3.6. N'-(1-(3-Methoxyphenylcarbamoyl)ethylidene)-4-(1H-pyrrol-1-yl)benzohydrazide

(12f)

Yield 68%; mp 98-100 °C; FTIR (KBr) cm^{-1}: 3248 (2° amine), 2937 (Ar-H), 1688, 1650 (C=O), 1590 (C=N); ^{1}H NMR (400 MHz, DMSO) δ ppm: 1.99 (s, 3H, -CH_3), 3.66 (s, 3H, -OCH_3), 6.34 (t, 2H, pyrrole-C_3, C_4-H), 6.80 (t, 1H, methoxyphenyl-C_4-H), 7.20-7.38 (m, 5H, pyrrole-C_2, C_5-H and methoxyphenyl-C_2, C_5, C_6-H), 7.48-7.52 (m, 2H, bridging phenyl-C_2, C_6-H), 7.64-7.70 (m, 2H, bridging phenyl-C_4, C_5-H), 9.10 (s, 1H, hydrazinylidene-NH), 10.03 (s, 1H, propanamide-NH); MS (ESI): m/z found 376.50 [M^+]; calcd. 376.15. Anal. Calcd. For $C_{21}H_{20}N_4O_3$: C, 67.01; H, 5.36; N, 14.88. Found: C, 67.17; H, 5.30; N, 14.89; UV-Visible λ_{max}: 317 nm.

4.3.7. N'-(1-(3-Fluorophenylcarbamoyl)ethylidene)-4-(1H-pyrrol-1-yl)benzohydrazide ***(12g)***

Yield 60%; mp 114-117°C; FTIR (KBr) cm^{-1}: 3241 (2° amine), 2932 (Ar-H), 1696, 1670 (C=O), 1601 (C=N); ^{1}H NMR (400 MHz, DMSO) δ ppm: 1.84 (s, 3H, -CH_3), 6.24 (t, 2H, pyrrole-C_3, C_4-H), 7.18 (t, 1H, fluorophenyl-C_4-H), 7.26 (t, 2H, pyrrole-C_2, C_5-H), 7.35 (t, 1H, fluoropheyl-C_5-H), 7.64 (t, 1H, fluoropheyl-C_6-H), 7.87 (t, 1H, fluorophenyl C_2, H), 7.93-7.96 (m, 2H, bridging phenyl-C_2, C_6-H), 7.99 (d, 2H, bridging phenyl-C_3, C_5-H), 10.34 (s, 1H, hydrazinylidene-NH), 11.04 (s, 1H, propanamide-NH); MS (ESI): m/z found 364.04 [M^+]; calcd. 364.13. Anal. Calcd. For $C_{20}H_{17}N_4O_2F$: C, 65.93; H, 4.70; N, 15.38. Found: C, 65.70; H, 4.68; N, 15.31; UV-Visible λ_{max}: 291 nm.

4.3.8. N'-(1-(4-Fluorophenylcarbamoyl)ethylidene)-4-(1H-pyrrol-1-yl)benzohydrazide ***(12h)***

Yield 71%; mp 87-89°C; FTIR (KBr) cm^{-1}: 3261 (2° amine), 2940 (Ar-H), 1680, 1674 (C=O), 1610 (C=N); ^{1}H NMR (400 MHz, DMSO) δ ppm: 1.86 (s, 3H, -CH_3), 6.25 (t, 2H, pyrrole-C_3, C_4-H), 7.18 (t, 2H, fluoropheyl-C_3, C_5-H), 7.38 (t, 2H, pyrrole-C_2, C_5-H), 7.94-7.98 (m, 4H, fluorophenyl-C_2, C_6-H and bridging phenyl-C_2, C_6-H), 8.21 (d, 2H, bridging phenyl-C_3, C_5-H), 10.36 (s, 1H, hydrazinylidene-NH), 11.06 (s, 1H, propanamide-NH); ^{13}C NMR (75 MHz, DMSO) δ ppm: 11.5, 111.1, 118.3, 118.4, 118.6, 121.5, 122.2, 126, 129.1, 130, 130.1, 139.7, 142.6, 153.8, 162.5; MS (ESI): m/z found 364.65 [M^+]; calcd. 364.13. Anal. Calcd. For $C_{20}H_{17}N_4O_2F$: C, 65.93; H, 4.70; N, 15.38. Found: C, 65.72; H, 4.64; N, 15.34; UV-Visible λ_{max}: 287 nm.

4.3.9. N'-(1-(2-Fluorophenylcarbamoyl)ethylidene)-4-(1H-pyrrol-1-yl)benzohydrazide ***(12i)***

Yield 54%; mp 107-109°C; FTIR (KBr) cm^{-1}: 3345 (2° amine), 2934 (Ar-H), 1694, 1677 (C=O); ^{1}H NMR (400 MHz, DMSO) δ ppm: 1.81 (s, 3H, -CH_3), 6.20 (t, 2H, pyrrole C_3, C_4, H), 7.10 (t, 1H, fluorophenyl-C_4-H), 7.33 (m, 4H, fluorophenyl-C_3, C_5 and pyrrole-C_2, C_5-H), 7.84 (d, 2H, bridging phenyl-C_2, C_6-H), 7.90 (t, 1H, fluorophenyl-C_6-H), 7.96 (d, 2H, bridging phenyl-C_3, C_5-H), 10.32 (s, 1H, hydrazinylidene-NH), 11.00 (s, 1H, propanamide-

NH); MS (ESI): m/z found 364.36 [M^+]; calcd. 364.13. Anal. Calcd. For $C_{20}H_{17}N_4O_2F$: C, 65.93; H, 4.70; N, 15.38. Found: C, 65.80; H, 4.71; N, 15.36; UV-Visible λ_{max}: 331 nm.

4.3.10. N-(3,5-Dibromophenyl)-2-{2-[4-(1H-pyrrol-1-yl)benzoyl]hydrazinylidene} propanamide ***(12j)***

Yield 54%; mp 170-174°C; FTIR (KBr) cm^{-1}: 3245 (2° amine), 2900 (Ar-H), 1714, 1680 (C=O), 1579 (C=N); ^{1}H NMR (400 MHz, DMSO) δ ppm: 1.84 (s, 3H, -CH_3), 6.20 (t, 2H, pyrrole-C_3, C_4-H), 6.91 (t, 2H, pyrrole-C_2, C_5-H), 7.54-7.60 (m, 5H, bridging phenyl-C_2, C_6-H and bromophenyl-C_2, C_4, C_6-H), 7.84 (d, 2H, bridging phenyl-C_2, C_6-H), 7.94 (d, 2H, bridging phenyl-C_3, C_5-H), 9.10 (s, 1H, hydrazinylidene -NH), 11.12 (s, 1H, propanamide -NH); ^{13}C NMR (75 MHz, DMSO) δ ppm: 11.5, 111.4, 118.2, 118.6, 118.7, 121.7, 121.1, 126.4, 129.2, 130.4, 130.7, 139.2, 142.4, 153.5, 162.8; MS (ESI): m/z found 504.14, 506.12, 508.24 [M^+, M^{+2}, M^{+4} (1:2:1)]; calcd. 504.17. Anal. Calcd. For $C_{20}H_{16}N_4O_2Br_2$: C, 47.64; H, 3.20; N, 11.11.Found: C, 47.60; H, 3.22; N, 11.10; UV-Visible λ_{max}: 279 nm.

4.3.11. N-(4-Bromophenyl)-4-{2-[4-(1H-pyrrol-1-yl)benzoyl]hydrazinylidene}pentanamide ***(12k)***

Yield 74%; mp 242-246°C; FTIR (KBr) cm^{-1}: 3278 (2° amine), 2923 (Ar-H), 1684, 1644 (C=O), 1610 (C=O); ^{1}H NMR (400 MHz, DMSO) δ ppm: 1.24 (s, 3H, -CH_3), 2.53 (t, 4H, pentamide-H), 6.28-6.30 (m, 2H, pyrrole-C_3, C_4-H), 7.36 (d, 2H, pyrrole-C_2, C_5-H), 7.60-7.66 (q, 4H, bromophenyl-C_2, C_3, C_5, C_6-H), 7.94 (d, 2H, bridging phenyl-C_2, C_6-H), 8.01-8.19 (m, 2H, bridging phenyl-C_3, C_5-H), 9.79 (s, 1H, hydrazinylidene -NH), 10.05 (s, 1H, pentanamide-NH); ^{13}C NMR (75 MHz, DMSO) δ ppm: 11.5, 30.1, 110.9, 111, 118.4, 118.7, 118.8, 128.5, 129.1, 129.5, 141.7, 159.6, 165.1; MS (ESI): m/z found 452.02, 454.17 [M^+, M^{+2} (1:1)]; calcd. 452.08. Anal. Calcd. For $C_{22}H_{21}N_4O_2Br$: C, 58.29; H, 4.67; N, 12.36. Found: C, 57.97; H, 4.62; N, 12.34; UV-Visible λ_{max}: 330 nm.

4.3.12. N-(3-Bromophenyl)-4-{2-[4-(1H-pyrrol-1-yl)benzoyl]hydrazinylidene}pentanamide

(12l)

Yield 72%; mp 234-236°C; FTIR (KBr) cm^{-1}: 3241 (2° amine), 2924 (Ar-H), 1693, 1660 (C=O), 1591 (C=N); ^{1}H NMR (400 MHz, DMSO) δ ppm: 1.30 (s, 3H, -CH_3), 2.54-2.55 (m, 4H, pentamide-H), 6.28-6.31 (m, 2H, pyrrole-C_3, C_4-H), 7.28-7.32 (m, 5H, pyrrole-C_2,C_5-H and bromophenyl-C_5, C_6-H), 7.53-7.59 (m, 1H, bromophenyl-C_4-H), 7.93-8.19 (m, 5H, bridging phenyl-C_2, C_3, C_5, C_6, H and bromophenyl C_2 -H), 9.78 (s, 1H, hydrazinylidene-NH), 9.99 (s, 1H, pentanamide-NH); ^{13}C NMR (75 MHz, DMSO) δ ppm: 20, 30.8, 110.9, 111, 118.3, 118.4, 118.7, 128.5, 129.1, 141.7; MS (ESI): m/z found 452.18, 454.14 [M^+, M^{+2} (1:1)]; calcd. 452.08. Anal. Calcd. For $C_{22}H_{21}N_4O_2Br$: C, 58.14; H, 4.64; N, 12.30. Found: C, 58.29; H, 4.67; N, 12.36; UV-Visible λ_{max}: 295 nm.

4.3.13. N-(2-Chlorophenyl)-4-{2-[4-(1H-pyrrol-1-yl)benzoyl]hydrazinylidene}pentanamide

(12m)

Yield 68%; mp 244-248°C; FTIR (KBr) cm^{-1}: 3241 (2° amine), 2923 (Ar-H), 1694, 1644 (C=O), 1588 (C=N); ^{1}H NMR (400 MHz, DMSO) δ ppm: 1.94 (s, 3H, -CH_3), 2.50-2.52 (m, 4H, pentamide-H), 6.28-6.30 (m, 2H, pyrrole C_3, C_4, H), 7.40-7.44 (m, 4H, chlorophenyl-C_4, C_5-H and pyrrole-C_2,C_5-H), 7.62-7.71 (m, 1H, chlorophenyl-C_3-H), 7.91-7.98 (q, 2H, bridging phenyl-C_2, C_6-H), 8.25 (s, 3H, chlorophenyl-C_6-H and bridging phenyl-C_3, C_5-H), 9.88 (s, 1H, hydrazinylidene-NH), 10.30 (s, 1H, pentanamide-NH); MS (ESI): m/z found 408.06, 410.14 [M^+, M^{+2} (3:1)]; calcd. 408.14. Anal. Calcd. For $C_{22}H_{21}N_4O_2Cl$: C, 64.62; H, 5.18; N, 13.70. Found: C, 64.47; H, 5.16; N, 13.72; UV-Visible λ_{max}: 280 nm.

4.3.14. N-(3-Chlorophenyl)-4-{2-[4-(1H-pyrrol-1-yl)benzoyl]hydrazinylidene}pentanamide

(12n)

Yield 67%; mp 249-251°C; FTIR (KBr) cm^{-1}: 3245 (2° amine), 2924 (Ar-H), 1692, 1644 (C=O), 1590 (C=N); ^{1}H NMR (400 MHz, DMSO) δ ppm: 1.94 (s, 3H, -CH_3), 2.51-2.52 (m,

4H, pentamide-H), 6.29-6.31 (m, 2H, pyrrole-C_3, C_4-H), 7.41-7.45 (m, 3H, pyrrole-C_2,C_5 and chlorophenyl-C_4-H), 7.65-8.23 (m, 7H, chlorophenyl-C_2, C_5, C_6-H and bridging phenyl-C_2, C_3, C_5, C_6-H), 9.88 (s, 1H, hydrazinylidene-NH), 10.30 (s, 1H, pentanamide-NH); MS (ESI): m/z found 408.14, 410.18 [M^+, M^{+2} (3:1)]; calcd. 408.14. Anal. Calcd. For $C_{22}H_{21}N_4O_2Cl$: C, 64.62; H, 5.18; N, 13.70. Found: C, 64.39; H, 5.14; N, 13.71; UV-Visible λ_{max}: 310 nm.

4.3.15. N-(4-Chlorophenyl)-4-{2-[4-(1H-pyrrol-1-yl)benzoyl]hydrazinylidene}pentanamide ***(12o)***

Yield 67%; mp 250-252°C; FTIR (KBr) cm^{-1}: 3234 (2° amine), 3035 (Ar-H), 1693, 1644 (C=O), 1590 (C=N); ^{1}H NMR (400 MHz, DMSO) δ ppm: 1.98 (s, 3H, -CH_3), 2.51-2.56 (m, 4H, pentamide-H), 6.29 (t, 2H, pyrrole-C_3, C_4-H), 7.43 (t, 2H, pyrrole-C_2, C_5-H), 7.72 (dd, 2H, chlorophenyl-C_3, C_5-H), 7.96-8.11 (m, 4H, chlorophenyl-C_2, C_6 and bridging phenyl-C_2, C_6-H), 8.23 (s, 2H, bridging phenyl-C_3, C_5-H), 9.94 (s, 1H, hydrazinylidene-NH), 10.40 (s, 1H, pentanamide-NH); MS (ESI): m/z found 408.47, 410.25 [M^+, M^{+2} (3:1)]; calcd. 408.14. Anal. Calcd. For $C_{22}H_{21}N_4O_2Cl$: C, 64.62; H, 5.18; N, 13.70. Found: C, 64.67; H, 5.15; N, 13.72; UV-Visible λ_{max}: 287 nm.

4.3.16. N-(3,5-Dichlorophenyl)-4-{2-[4-(1H-pyrrol-1-yl)benzoyl]hydrazinylidene} pentanamide ***(12p)***

Yield 58%; mp 201-203°C; FTIR (KBr) cm^{-1}: 3325 (2° amine), 3015 (Ar-H), 1697, 1667 (C=O), 1618 (C=N); ^{1}H NMR (400 MHz, DMSO) δ ppm: 1.98 (s, 3H, -CH_3), 2.51-2.56 (m, 4H, pentamide-H), 6.30 (t, 2H, pyrrole-C_3, C_4-H), 7.20 (t, 2H, pyrrole-C_2, C_5-H), 7.41 (t, 1H, chlorophenyl-C_4-H), 7.72 (m, 2H, chlorophenyl-C_2, C_6 and bridging phenyl-C_2, C_6-H), 7.96 (d, 2H, bridging phenyl-C_3, C_5-H), 9.88 (s, 1H, hydrazinylidene-NH), 10.54 (s, 1H, pentanamide-NH); MS (ESI): m/z found 444 [M^{+1}]; calcd. 443.33. Anal. Calcd. For $C_{22}H_{20}N_4O_2Cl_2$: C, 59.60; H, 4.55; N, 12.64. Found: C, 60.67; H, 5.15; N, 13.72; UV-Visible λ_{max}: 286 nm.

4.3.17. N'-(4-(2-Methoxyphenylcarbamoyl)butan-2-ylidene)-4-(1H-pyrrol-1-yl) benzohydrazide ***(12q)***

Yield 61%; mp 88-90°C; FTIR (KBr) cm^{-1}: 3314 (2° amine), 3014 (Ar-H), 1702, 1687 (C=O), 1608 (C=N); ^{1}H NMR (400 MHz, DMSO) δ ppm: 1. 84 (s, 3H, -CH_3), 2.02-2.08 (m, 4H, pentamide-H), 3.22 (s, 3H, -OCH_3), 6.29 (t, 2H, pyrrole-C_3, C_4-H), 6.89-7.22 (m, 5H, methoxyphenyl-C_3, C_4, C_5 and pyrrole-C_2, C_5-H), 7.72 (m, 3H, methoxyphenyl-C_6 and bridging phenyl-C_2, C_6-H), 8.11 (d, 2H, bridging phenyl-C_3, C_5-H), 9.69 (s, 1H, hydrazinylidene-NH), 10.49 (s, 1H, pentanamide-NH); UV-Visible λ_{max}: 284 nm.

4.3.18. N'-(4-(4-Fluorophenylcarbamoyl)butan-2-ylidene)-4-(1H-pyrrol-1-yl)benzohydrazide (***12r***)

Yield 71%; mp 140-142°C; FTIR (KBr) cm^{-1}: 3274 (2° amine), 2924 (Ar-H), 1701, 1687 (C=O), 1577 (C=N); ^{1}H NMR (400 MHz, DMSO) δ ppm: 1.98 (s, 3H, -CH_3), 2.51-2.56 (m, 4H, pentamide-H), 6.29 (t, 2H, pyrrole-C_3, C_4-H), 7.28-7.32 (m, 4H, pyrrole-C_2, C_5 and fluorophenyl-C_3, C_5-H), 7.72 (d, 2H, fluorophenyl-C_2, C_6-H), 7.96-8.01 (m, 2H, bridging phenyl-C_2, C_6-H), 8.23 (s, 2H, bridging phenyl-C_3, C_5-H), 9.88 (s, 1H, hydrazinylidene-NH), 10.54 (s, 1H, pentanamide-NH); MS (ESI): m/z found 392.64 [M^+]; calcd. 392.16 Anal. Calcd. For $C_{22}H_{21}N_4O_2F$: C, 67.37; H, 5.35; N, 14.24. Found: C, 67.27; H, 5.37; N, 14.26; UV-Visible λ_{max}: 282 nm.

4.3.19. N'-(4-(3-Fluorophenylcarbamoyl)butan-2-ylidene)-4-(1H-pyrrol-1-yl)benzohydrazide (***12s***)

Yield 64%; mp 120-122°C; FTIR (KBr) cm^{-1}: 3241 (2° amine), 2942 (Ar-H), 1707, 1685 (C=O), 1579 (C=N); ^{1}H NMR (400 MHz, DMSO) δ ppm: 1.74 (s, 3H, -CH_3), 2.63-2.69 (m, 4H, pentamide-H), 6.35 (t, 2H, pyrrole-C_3, C_4-H), 7.38 (t, 3H, pyrrole-C_2, C_5 and fluoro phenyl-C_4-H), 7.47 (t, 2H, fluorophenyl-C_5, C_6-H), 7.73 (t, 3H, flurophenyl-C_2 and bridging phenyl-C_2, C_6-H), 8.07 (t, 2H, bridging phenyl-C_3, C_5-H), 10.43 (s, 1H, hydrazinylidene-NH),

11.15 (s, 1H, pentanamide-NH); MS (ESI): m/z found 392.64 [M^+]; calcd. 392.16 Anal. Calcd. For $C_{22}H_{21}N_4O_2F$: C, 67.37; H, 5.35; N, 14.24. Found: C, 67.27; H, 5.37; N, 14.26; UV-Visible λ_{max}: 285 nm.

4.3.20. N'-(4-(2-Fluorophenylcarbamoyl)butan-2-ylidene)-4-(1H-pyrrol-1-yl)benzohydrazide (***12t***)

Yield 52%; mp 89-91°C; FTIR (KBr) cm^{-1}: 3285 (2° amine), 2961 (Ar-H), 1692, 1670 (C=O), 1611 (C=N); ^{1}H NMR (400 MHz, DMSO) δ ppm: 1.78 (s, 3H, -CH_3), 2.34 (m, 4H, pentamide-H), 6.31 (t, 2H, pyrrole-C_3, C_4-H), 6.90-7.26 (m, 5H, pyrrole-C_2, C_5-H and fluorophenyl-C_3, C_4, C_5-H), 7.82 (t, 2H, bridging phenyl-C_2, C_6-H), 8.00 (t, 1H, flurophenyl-C_6-H), 8.12 (d, 2H, bridging phenyl-C_3, C_5-H), 10.31 (s, 1H, hydrazinylidene-NH), 11.04 (s, 1H, pentanamide-NH); MS (ESI): m/z found 392.60 [M^+]; calcd. 392.16 Anal. Calcd. For $C_{22}H_{21}N_4O_2F$: C, 67.40; H, 5.36; N, 14.25. Found: C, 67.27; H, 5.37; N, 14.26; UV-Visible λ_{max}: 275 nm.

4.3.21. N'-(4-(phenylcarbamoyl)butan-2-ylidene)-4-(1H-pyrrol-1-yl)benzohydrazide ***(12u)***

Yield 78%; mp 93-95 °C; FTIR (KBr) cm^{-1}: 3276 (2° amine), 2940 (Ar-H), 1680, 1674 (C=O), 1579 (C=N); ^{1}H NMR (400 MHz, DMSO) δ ppm: 1.72 (s, 3H, -CH_3), 2.53-2.54 (m, 4H, pentamide-H), 6.24 (t, 2H, pyrrole C_3, C4, H), 7.20 (t, 3H, pyrrole-C_2, C_5 and phenyl-C_4-H), 7.34 (d, 2H, phenyl-C_3, C_5-H), 7.48 (d, 2H, phenyl-C_2, C_6-H), 7.50 (t, 2H, bridging phenyl-C_2, C_6-H), 7.71 (t, 2H, bridging phenyl-C_3, C_5-H), 10.25 (s, 1H, hydrazinylidene-NH), 10.51 (s, 1H, pentanamide-NH); MS (ESI): m/z found 374.47 [M^+]; calcd. 374.17 Anal. Calcd. For $C_{22}H_{22}N_4O_2$: C, 70.57; H, 5.92; N, 14.96;. Found: C, 70.50; H, 5.90; N, 14.94; UV-Visible λ_{max}: 327 nm.

4.3.22. N'-(1-(4-Bromophenylcarbamoyl)ethylidene)-4-(2,5-dimethyl-1H-pyrrol-1-yl) benzohydrazide ***(12v)***

Yield 70%; mp 128-130°C; FTIR (KBr) cm^{-1}: 3274 (2° amine), 3074 (Ar-H), 1692, 1665 (C=O), 1590 (C=N); ^{1}H NMR (400 MHz, DMSO) δ ppm: 2.10 (s, 6H, 2-CH_3), 2.31 (s, 3H, -CH_3), 5.98 (s, 2H, pyrrole-C_3, C_4-H), 7.28-8.00 (m, 8H, bridging phenyl-C_2, C_3, C_5, C_6 and bromophenyl- C_2, C_3, C_5, C_6-H), 9.00 (s, 1H, hydrazinylidene-NH), 9.42 (s, 1H, propanamide-NH); ^{13}C NMR (75 MHz, DMSO) δ ppm: 12.7, 22.7, 106.8, 114.1. 116.9, 121.6, 128.5, 131.9, 135.3, 143, 160, 175; MS (ESI): m/z found 437.23, 439.35 [M^+, M^{+2} (1:1)]; calcd. 437.07. Anal. Calcd. For $C_{22}H_{20}BrN_3O_2$: C, 60.28; H, 4.60; N, 9.59; Found: C, 60.24; H, 4.64; N, 9.57; UV-Visible λ_{max}: 320 nm.

4.3.23. N-(2,6-Dichlorophenyl)-2-{2-[4-(2,5-dimethyl-1H-pyrrol-1yl)benzoyl] hydrazinylidene}propanamide ***(12w)***

Yield 61%; mp 180-182°C; FTIR (KBr) cm^{-1}: 3254 (2° amine), 2923 (Ar-H), 1662, 1646 (C=O), 1594 (C=N); ^{1}H NMR (400 MHz, DMSO) δ ppm: 1.99 (s, 6H, 2-CH_3), 2.53 (t, 3H, -CH_3), 5.80 (s, 2H, pyrrole C_3, C_4, H), 6.70 (s, 1H, chlorophenyl-C_4-H), 7.01 (d, 2H, chlorophenyl-C_3, C_5-H), 7.30 (d, 2H, bridging phenyl-C_2, C_6-H), 7.97 (d, 2H, bridging phenyl-C_3, C_5-H), 9.88 (s, 1H, hydrazinylidene-NH), 10.28 (s, 1H, propanamide-NH); MS (ESI): m/z found 442.01, 444.15, 446.25 [M^+, M^{+2}, M^{+4} (9:6:1)]; calcd. 442.21. Anal. Calcd. For $C_{22}H_{20}N_4O_2Cl_2$: C, 59.51; H, 4.54; N, 12.65. Found: C, 59.60; H, 4.55; N, 12.64; UV-Visible λ_{max}: 254 nm.

4.3.24. N'-(1-(4-Methoxyphenylcarbamoyl)ethylidene)-4-(2,5-dimethyl-1H-pyrrol-1-yl) benzohydrazide ***(12x)***

Yield 72%; mp 94-96°C; FTIR (KBr) cm^{-1}: 3281 (2° amine), 2953 (Ar-H), 1692, 1666 (C=O), 1608 (C=N); ^{1}H NMR (400 MHz, DMSO) δ ppm: 1.19 (s, 6H, -CH_3), 2.53 (s, 3H, -CH_3), 3.63 (s, 3H, -OCH_3), 5.82 (t, 2H, pyrrole-C_3, C_4-H), 7.23 (t, 2H, methoxyphenyl-C_3, C_5-H), 7.40 (t, 2H, methoxyphenyl-C_2, C_6-H), 7.53-7.56 (m, 2H, bridging phenyl-C_2, C_6-H), 7.70-7.79 (m, 2H, bridging phenyl-C_3, C_5-H), 9.12 (s, 1H, hydrazinylidene-NH), 10.00 (s,

1H, propanamide-NH); MS (ESI): m/z found 404.85 [M^+]; calcd. 404.18. Anal. Calcd. For $C_{23}H_{24}N_4O_3$: C, 68.30; H, 5.98; N, 13.85. Found: C, 68.24; H, 5.94; N, 13.83; UV-Visible λ_{max}: 318 nm.

4.3.25. 2-{2-[4-(1H-pyrrol-1-yl)benzoyl]hydrazinylidene}propanamide ***(12y)***

Yield 67%; mp 138-140°C; FTIR (KBr) cm^{-1}: 3331 (1° amine), 2926 (Ar-H), 1701, 1687 (C=O), 1588 (C=N); ^{1}H NMR (400 MHz, DMSO) δ ppm: 2.04 (s, 3H, -CH_3), 4.31 (s, 2H, -NH_2), 6.31 (t, 2H, pyrrole-C_3, C_4-H), 7.19-7.22 (m, 2H, pyrrole-C_2, C_5-H), 7.46 (d, 2H, phenyl-C_2, C_6-H), 7.95 (d, 2H, phenyl-C_3, C_5-H), 9.70 (s, 1H, hydrazinylidene-NH); ^{13}C NMR (75 MHz, DMSO) δ ppm: 10.3, 110.8, 118.4, 118.7, 128.5, 129.5, 141.7, 165.1; MS (ESI): m/z found 270.27 [M^+]; calcd. 270.29. Anal. Calcd. For $C_{22}H_{21}N_4O_2Br$: C, 62.21; H, 5.22; N, 20.73. Found: C, 62.05; H, 5.21; N, 20.72; UV-Visible λ_{max}: 282 nm.

*4.3. General procedure for synthesis of copper complexes (**13a-y**)*

Copper(II) acetate monohydrate (1 mol) and ligand (**12a-y**) (2 mol) were refluxed in dry methanol (30 mL) for 58-60 h. The complexes formed was filtered off and washed with cold methanol. The crude product was dried and crystals were formed by recrystalization using methanol.

4.4.1. (bis)[N-(3-Bromophenyl)-2-{2-[4-(1H-pyrrol-1-yl)benzoyl]hydrazinylidene} propanamide]copper(II)anhydride ***(13a)***

Yield 62%, green solid, mp 290-292 °C; FTIR (KBr) cm^{-1}: $\upsilon_{(C=N)}$ 1663, $\upsilon_{(C=N)}$ 1604; MS (ESI): m/z found 910.25, 912.14, 914.58 [M^+, M^{+2}, M^{+4} (1:2:1)]; calcd. 910.07. Anal. Calcd. For $C_{40}H_{30}Br_2CuN_8O_4$: C, 52.79; H, 3.32; N, 12.31; Found: C, 52.75; H, 3.31; N, 12.30; UV-Visible λ_{max}: 675 nm.

4.4.2. (bis)[N-(4-Bromophenyl)-2-{2-[4-(1H-pyrrol-1-yl)benzoyl]hydrazinylidene} propanamide]copper (II)anhydride ***(13b)***

Yield 68%, green solid, mp 315-317 °C; FTIR (KBr) cm^{-1}: $\upsilon_{(C=N)}$ 1633, $\upsilon_{(C=N)}$ 1605; MS (ESI): m/z found 910.54, 912.01, 914.46 [M^+, M^{+2}, M^{+4} (1:2:1)]; calcd. 910.07. Anal. Calcd. For $C_{40}H_{30}Br_2CuN_8O_4$: C, 52.79; H, 3.32; N, 12.31; Found: C, 52.70; H, 3.34; N, 12.32; UV-Visible λ_{max}: 610 nm.

4.4.3. (bis)[N-(2,6-Dichlorophenyl)-2-{2-[4-(1H-pyrrol-1-yl)benzoyl]hydrazinylidene} propanamide]copper(II)anhydride ***(13c)***

Yield 48%, green solid, mp 236-238 °C; FTIR (KBr) cm^{-1}: $\upsilon_{(C=N)}$ 1668, $\upsilon_{(C=N)}$ 1621; MS (ESI): m/z found 891.04, 893.16, [M^+, M^{+2}]; calcd. 890.06 Anal. Calcd. For $C_{40}H_{28}Cl_4CuN_8O_4$: C, 53.98; H, 3.17; N, 12.59; Found: C, 53.95; H, 3.15; N, 12.57; UV-Visible λ_{max}: 717 nm.

4.4.4. (bis)[N-(3,5-Dichlorophenyl)-2-{2-[4-(1H-pyrrol-1-yl)benzoyl]hydrazinylidene} propanamide]copper(II)anhydride ***(13d)***

Yield 52%, green solid, mp 313-315 °C; FTIR (KBr) cm^{-1}: $\upsilon_{(C=N)}$ 1658, $\upsilon_{(C=N)}$ 1626; MS (ESI): m/z found 890.47, 892.29, [M^+, M^{+2}]; calcd. 890.06 Anal. Calcd. For $C_{40}H_{28}Cl_4CuN_8O_4$: C, 53.98; H, 3.17; N, 12.59; Found: C, 53.91; H, 3.14; N, 12.56; UV-Visible λ_{max}: 719 nm.

4.4.5. (bis)[N'-(1-(4-Methoxyphenylcarbamoyl)ethylidene)-4-(1H-pyrrol-1-yl) benzohydrazide]copper(II)anhydride ***(13e)***

Yield 68%, green solid, mp 256-258 °C; FTIR (KBr) cm^{-1}: $\upsilon_{(C=N)}$ 1650, $\upsilon_{(C=N)}$ 1615; MS (ESI): m/z found 812.58 [M^+]; calcd. 812.33 Anal. Calcd. For $C_{42}H_{36}CuN_8O_6$: C, 62.10; H, 4.47; N, 13.79; Found: C, 61.96; H, 4.44; N, 13.76; UV-Visible λ_{max}: 672 nm.

4.4.6. (bis)[N'-(1-(3-Methoxyphenylcarbamoyl)ethylidene)-4-(1H-pyrrol-1-yl) benzohydrazide]copper(II)anhydride ***(13f)***

Yield 53%, green solid, mp 243-245 °C; FTIR (KBr) cm^{-1}: $\upsilon_{(C=N)}$ 1661, $\upsilon_{(C=N)}$ 1623; MS (ESI): m/z found 812.97 [M^+]; calcd. 812.33 Anal. Calcd. For $C_{42}H_{36}CuN_8O_6$: C, 62.10; H, 4.47; N, 13.79; Found: C, 62.21; H, 4.48; N, 13.78; UV-Visible λ_{max}: 698 nm.

4.4.7. (bis)[N'-(1-(3-Fluorophenylcarbamoyl)ethylidene)-4-(1H-pyrrol-1-yl)benzohydrazide]copper(II)anhydride ***(13g)***

Yield 52%, green solid, mp 321-323 °C; FTIR (KBr) cm^{-1}: $\upsilon_{(C=N)}$ 1662, $\upsilon_{(C=N)}$ 1624; MS (ESI): m/z found 788.54, [M^+]; calcd. 788.26 Anal. Calcd. For $C_{40}H_{30}CuF_2N_8O_6$: C, 60.95; H, 3.84; N, 14.22; Found: C, 60.62; H, 3.81; N, 14.20; UV-Visible λ_{max}: 681 nm.

4.4.8. (bis)[N'-(1-(4-Fluorophenylcarbamoyl)ethylidene)-4-(1H-pyrrol-1-yl)benzohydrazide]copper(II)anhydride ***(13h)***

Yield 52%, green solid, mp 328-330 °C; FTIR (KBr) cm^{-1}: $\upsilon_{(C=N)}$ 1675, $\upsilon_{(C=N)}$ 1641; MS (ESI): m/z found 788.62, [M^+]; calcd. 788.26 Anal. Calcd. For $C_{40}H_{30}CuF_2N_8O_6$: C, 60.95; H, 3.84; N, 14.22; Found: C, 60.81; H, 3.87; N, 14.21; UV-Visible λ_{max}: 641 nm.

4.4.9. (bis)[N'-(4-(2-Fluorophenylcarbamoyl)butan-2-ylidene)-4-(1H-pyrrol-1-yl) benzohydrazide]copper(II)anhydride ***(13i)***

Yield 46%, green solid, mp 234-236 °C; FTIR (KBr) cm^{-1}: $\upsilon_{(C=N)}$ 1661, $\upsilon_{(C=N)}$ 1632; MS (ESI): m/z found 844.41, [M^+]; calcd. 844.37 Anal. Calcd. For $C_{44}H_{38}CuF_2N_8O_6$: C, 62.59; H, 4.54; N, 13.27; Found: C, 62.35; H, 4.53; N, 13.24; UV-Visible λ_{max}: 659 nm.

4.4.10. (bis)[N-(3,5-Dibromophenyl)-2-{2-[4-(1H-pyrrol-1-yl)benzoyl]hydrazinylidene} propanamide]copper(II)anhydride ***(13j)***

Yield 48%, green solid, mp 341-343 °C; FTIR (KBr) cm^{-1}: $\upsilon_{(C=N)}$ 1679, $\upsilon_{(C=N)}$ 1648; MS (ESI): m/z found 1067.54, [M^+]; calcd. 1067.86 Anal. Calcd. For $C_{40}H_{28}CuBr_4N_8O_4$: C, 44.99; H, 2.64; N, 10.49; Found: C, 44.91; H, 2.62; N, 10.45; UV-Visible λ_{max}: 673 nm.

4.4.11. (bis)[N-(4-Bromophenyl)-4-{2-[4-(1H-pyrrol-1-yl)benzoyl]hydrazinylidene} pentanamide]copper(II) anhydride ***(13k)***

Yield 65%, green solid, mp 275-277 °C; FTIR (KBr) cm^{-1}: $\upsilon_{(C=N)}$ 1677, $\upsilon_{(C=N)}$ 1608; MS (ESI): m/z found 966.46, 968.04, 970.25 [M^+, M^{+2}, M^{+4} (1:2:1)]; calcd. 966.18 Anal. Calcd. For $C_{44}H_{38}Br_2CuN_8O_4$: C, 54.70; H, 3.96; N, 11.60; Found: C, 54.76; H, 3.94; N, 11.62; UV-Visible λ_{max}: 645 nm.

4.4.12. (bis)[N-(3-Bromophenyl)-4-{2-[4-(1H-pyrrol-1-yl)benzoyl]hydrazinylidene} pentanamide]copper(II)anhydride ***(13l)***

Yield 63%, green solid, mp 263-265 °C; FTIR (KBr) cm^{-1}: $\upsilon_{(C=N)}$ 1663, $\upsilon_{(C=N)}$ 1608; MS (ESI): m/z found 966.62, 968.00, 970.41 [M^+, M^{+2}, M^{+4} (1:2:1)]; calcd. 966.18 Anal. Calcd. For $C_{44}H_{38}Br_2CuN_8O_4$: C, 54.70; H, 3.96; N, 11.60; Found: C, 54.79; H, 3.99; N, 11.61; UV-Visible λ_{max}: 666 nm.

4.4.13. (bis)[N-(2-Chlorophenyl)-4-{2-[4-(1H-pyrrol-1-yl)benzoyl]hydrazinylidene} pentanamide]copper(II)anhydride ***(13m)***

Yield 52%, green solid, mp 271-273 °C; FTIR (KBr) cm^{-1}: $\upsilon_{(C=N)}$ 1669, $\upsilon_{(C=N)}$ 1607; MS (ESI): m/z found 877.45, 879.00, 881.31 [M^+, M^{+2}, M^{+4} (9:6:1)]; calcd. 877.28 Anal. Calcd. For $C_{44}H_{38}Cl_2CuN_8O_4$: C, 60.24; H, 4.37; N, 12.77; Found: C, 60.21; H, 4.36; N, 12.75; UV-Visible λ_{max}: 678 nm.

4.4.14. (bis)[N-(3-Chlorohenyl)-4-{2-[4-(1H-pyrrol-1-yl)benzoyl]hydrazinylidene} pentanamide]copper (II)anhydride ***(13n)***

Yield 59%, green solid, mp 242-244 °C; FTIR (KBr) cm^{-1}: $\upsilon_{(C=N)}$ 1672, $\upsilon_{(C=N)}$ 1626; MS (ESI): m/z found 877.26, 879.14, 881.49 [M^+, M^{+2}, M^{+4} (9:6:1)]; calcd. 877.28 Anal. Calcd. For $C_{44}H_{38}Cl_2CuN_8O_4$: C, 60.24; H, 4.37; N, 12.77; Found: C, 60.14; H, 4.39; N, 12.75; UV-Visible λ_{max}: 681 nm.

4.4.15. (bis)[N-(4-Chlorohenyl)-4-{2-[4-(1H-pyrrol-1-yl)benzoyl]hydrazinylidene} pentanamide]copper (II)anhydride ***(13o)***

Yield 67%, green solid, mp 331-333 °C; FTIR (KBr) cm^{-1}: $\upsilon_{(C=N)}$ 1680, $\upsilon_{(C=N)}$ 1632; MS (ESI): m/z found 877.85, 879.94, 881.62 [M^+, M^{+2}, M^{+4} (9:6:1)]; calcd. 877.28 Anal. Calcd. For $C_{44}H_{38}Cl_2CuN_8O_4$: C, 60.24; H, 4.37; N, 12.77; Found: C, 60.29; H, 4.34; N, 12.74; UV-Visible λ_{max}: 710 nm.

4.4.16. (bis)[N-(3,5-Dichlorophenyl)-4-{2-[4-(1H-pyrrol-1-yl)benzoyl]hydrazinylidene} pentanamide]copper(II)anhydride ***(13p)***

Yield 49%, green solid, mp 301-303 °C; FTIR (KBr) cm^{-1}: $\upsilon_{(C=N)}$ 1662, $\upsilon_{(C=N)}$ 1614; MS (ESI): m/z found 946.43, 948.41, [M^+, M^{+2}]; calcd. 946.17 Anal. Calcd. For $C_{44}H_{36}Cl_4CuN_8O_4$: C, 55.85; H, 3.84; N, 11.84; Found: C, 55.81; H, 3.85; N, 11.81; UV-Visible λ_{max}: 664 nm.

4.4.17. (bis)[N'-(4-(2-Methoxyphenylcarbamoyl)butan-2-ylidene)-4-(1H-pyrrol-1-yl) benzohydrazide]copper(II)anhydride ***(13q)***

Yield 50%, green solid, mp 257-259 °C; FTIR (KBr) cm^{-1}: $\upsilon_{(C=N)}$ 1671, $\upsilon_{(C=N)}$ 1638; MS (ESI): m/z found 868.71 [M^+]; calcd. 868.44 Anal. Calcd. For $C_{46}H_{44}CuN_8O_6$: C, 63.62; H, 5.11; N, 12.90; Found: C, 63.57; H, 5.13; N, 12.87; UV-Visible λ_{max}: 721 nm.

4.4.18. (bis)[N'-(4-(4-Fluorophenylcarbamoyl)butan-2-ylidene)-4-(1H-pyrrol-1-yl) benzohydrazide]copper(II)anhydride ***(13r)***

Yield 50%, green solid, mp 313-316 °C; FTIR (KBr) cm^{-1}: $\upsilon_{(C=N)}$ 1670, $\upsilon_{(C=N)}$ 1645; MS (ESI): m/z found 844.59, [M^+]; calcd. 844.37 Anal. Calcd. For $C_{44}H_{38}CuF_2N_8O_6$: C, 62.59; H, 4.54; N, 13.27; Found: C, 62.31; H, 4.51; N, 13.25; UV-Visible λ_{max}: 728 nm.

4.4.19. (bis)[N'-(4-(3-Fluorophenylcarbamoyl)butan-2-ylidene)-4-(1H-pyrrol-1-yl) benzohydrazide] copper(II)anhydride ***(13s)***

Yield 54%, green solid, mp 256-259 °C; FTIR (KBr) cm^{-1}: $\upsilon_{(C=N)}$ 1674, $\upsilon_{(C=N)}$ 1642; MS (ESI): m/z found 844.24, [M^+]; calcd. 844.37 Anal. Calcd. For $C_{44}H_{38}CuF_2N_8O_6$: C, 62.59; H, 4.54; N, 13.27; Found: C, 62.37; H, 4.54; N, 13.22; UV-Visible λ_{max}: 731 nm.

4.4.20. (bis)[N'-(1-(2-Fluorophenylcarbamoyl)ethylidene)-4-(1H-pyrrol-1-yl) benzohydraziide]copper(II)anhydride ***(13t)***

Yield 51%, green solid, mp 321-323 °C; FTIR (KBr) cm^{-1}: $\upsilon_{(C=N)}$ 1672, $\upsilon_{(C=N)}$ 1635; MS (ESI): m/z found 788.84, $[M^+]$; calcd. 788.26 Anal. Calcd. For $C_{40}H_{30}CuF_2N_8O_6$: C, 60.95; H, 3.84; N, 14.22; Found: C, 60.95; H, 3.85; N, 14.28; UV-Visible λ_{max}: 659 nm.

4.4.21. (bis)[N'-(4-(Phenylcarbamoyl)butan-2-ylidene)-4-(1H-pyrrol-1-yl)benzohydrazide] copper(II)anhydride ***(13u)***

Yield 56%, green solid, mp 256-258 °C; FTIR (KBr) cm^{-1}: $\upsilon_{(C=N)}$ 1664, $\upsilon_{(C=N)}$ 1624; MS (ESI): m/z found 808.58, $[M^+]$; calcd. 808.39 Anal. Calcd. For $C_{44}H_{40}CuN_8O_4$: C, 65.37; H, 4.99; N, 13.86; Found: C, 65.91; H, 4.97; N, 13.84; UV-Visible λ_{max}: 738 nm.

4.4.22. (bis)[N'-(1-(4-Bromophenylcarbamoyl)ethylidene)-4-(2,5-dimethyl-1H-pyrrol-1-yl) benzohydraziide]copper (II)anhydride ***(13v)***

Yield 64%, green solid, mp 320-322 °C; FTIR (KBr) cm^{-1}: $\upsilon_{(C=N)}$ 1663, $\upsilon_{(C=N)}$ 1602; MS (ESI): m/z found 965.47, 967.01$[M^+, M^{+2}]$; calcd. 963.07. Anal. Calcd. For $C_{44}H_{38}Br_2CuN_8O_4$: C, 54.70; H, 3.96; N, 11.60; Found: C, 54.75; H, 3.94; N, 11.62; UV-Visible λ_{max}: 660 nm.

4.4.23. (bis)[N-(2,6-Dichlorophenyl)-2-{2-[4-(2,5-dimethyl-1H-pyrrol-1yl)benzoyl] hydrazinylidene}propanamide]copper(II)anhydride ***(13w)***

Yield 52%, green solid, mp 241-243 °C; FTIR (KBr) cm^{-1}: $\upsilon_{(C=N)}$ 1684, $\upsilon_{(C=N)}$ 1626; MS (ESI): m/z found 946.58, 948.12, $[M^+, M^{+2}]$; calcd. 946.17 Anal. Calcd. For $C_{44}H_{36}Cl_4CuN_8O_4$: C, 55.85; H, 3.84; N, 11.84; Found: C, 55.42; H, 3.81; N, 11.86; UV-Visible λ_{max}: 624 nm.

4.4.24. (bis)[N'-(1-(4-Methoxyphenylcarbamoyl)ethylidene)-4-(2,5-dimethyl-1H-pyrrol-1-yl)benzohydraziide]copper(II)anhydride ***(13x)***

Yield 47%, green solid, mp 242-244 °C; FTIR (KBr) cm^{-1}: $\upsilon_{(C=N)}$ 1668, $\upsilon_{(C=N)}$ 1635; MS (ESI): m/z found 868.54, $[M^+]$; calcd. 868.44 Anal. Calcd. For $C_{46}H_{44}CuN_8O_6$: C, 63.62; H, 5.11; N, 12.90; Found: C, 63.69; H, 5.15; N, 12.85; UV-Visible λ_{max}: 652 nm.

4.4.25. (bis)[2-{2-[4-(1H-pyrrol-1-yl)benzoyl]hydrazinylidene}propanamide]copper(II) anhydride ***(13y)***

Yield 60%, green solid, mp 280-283 °C; FTIR (KBr) cm^{-1}: $\upsilon_{(C=N)}$ 1678, $\upsilon_{(C=N)}$ 1606; MS (ESI): m/z found 599.14$[M^-]$; calcd. 600.9. Anal. Calcd. For $C_{28}H_{24}CuN_8O_4$: C, 56.04; H, 4.03; N, 18.65; Found: C, 56.00; H, 4.01; N, 18.64; UV-Visible λ_{max}: 670 nm.

5. BIOLOGY

5.1. Enzyme inhibition studies

5.1.1. InhA expression and purification

The production and purification of InhA-6xHis protein from a protease-deficient strain of *E. coli* (BL21) transformed with pHAT5/InhA plasmid were performed as follows. A 1 mL of bacteria was grown in 100 mL of Lysogeny broth (LB) medium containing ampicillin (100 µg/mL) and 2% glucose at 37°C. After 4 h, the solution was re-diluted in 1 L of the same medium and re-grown at 37°C. After reaching the proper concentration (OD_{595} = 0.6 - 0.8), the culture was centrifuged at 3300 g for 10 min at 4°C, and the bacteria were suspended in LB medium containing ampicillin (100 µg/mL). Protein expression was induced for overnight incubation in 1 mM isopropyl-*β*-D-galactopyranoside (IPTG) at 20°C. Cells were harvested by centrifugation at 6000 g for 30 min at 4°C. The dry pellet was kept at -80°C for several months and purification was performed with Ni-NTA Agarose from QIAGEN as described by the manufacturer's protocol. The purified recombinant protein was applied to PD-10 desalting columns (GE Healthcare, Piscataway, NJ) equilibrated with PIPES 30 mM pH 6.8, 150 mM NaCl to remove the imidazole. Samples were analyzed using SDS-PAGE and Coomassie blue staining and then stored at 4°C for short-term storage at -80 °C with 20% glycerin for long-term storage [46].

5.1.2. InhA activity inhibition

Triclosan and NADH were obtained from Sigma-Aldrich. Stock solutions of the selected compounds were prepared in DMSO such that the final concentration of this co-solvent was constant at 5% (v/v) in the final volume of 1 mL for all kinetic reactions. Kinetic assays were performed using *trans*-2-dodecenoyl-coenzyme A (DDCoA) and wild type InhA as previously described [47]. Briefly, reactions were performed at 25°C in an aqueous buffer (30 mM PIPES and 150 mM NaCl pH 6.8) containing 250 µM cofactor (NADH), 50 µM

substrate (DDCoA) and the test compound at 50 µM. Reactions were initiated by the addition of InhA (100 nM final) and NADH oxidation was monitored at the fixed 340 nm wavelength. Inhibitory activity of each derivative was expressed as % inhibition of InhA activity (initial velocity of the reaction) with respect to control reaction without the inhibitor.

% inhibition = slope (without inhibitor) - slope (with inhibitor) / slope (without inhibitor).

For the most efficient compounds, i.e. **13r**, **13b**, **12r**, IC50 values were determined using SciDAVIS software with at least six different concentrations of inhibitors as previously described. [48]

These results are shown in Table 7.

5.2.In vitro evaluation of antitubercular studies

All the compounds were tested for inhibition of *M. tuberculosis* strain H37RV using Microplate Alamar Blue Assay (MABA) as described earlier [49]. The 96 wells plate received 100 mL of Middlebrook 7H9 broth and serial dilution of compounds were made directly on the plate with drug concentrations of 0.2, 0.4, 0.8, 1.6, 3.125, 6.25,12.5, 25, 50 and 100 µg/mL. Plates were covered and sealed with parafilm and incubated at 37^{o}C for 5 days. Then, 25 mL of freshly prepared 1:1 mixture of almar blue reagent and 10% Tween 80 was added to the plate and incubated for 24 h. A blue color in the well was interpreted as no bacterial growth, while pink color was scored as the growth. The MIC was defined as the lowest drug concentration, which prevented the color change from blue to pink. Table 1 reveals the anti-TB activity data expressed in MIC.

5.3. MTT-based cytotoxicity activity

Cellular conversion of MTT [3-(4,5-dimethylthiazo-2-yl)-2,5-diphenyl-tetrazolium bromide] into a formazan product [50] was used to evaluate the cytotoxic activity (IC_{50}) of some of the compounds against A549 (lung adenocarcinoma) cell-line up to a concentrations of 50 mg/mL using Promega Cell Titer 96 non-radioactive cell proliferation assay [51] with

cisplatin as the positive control. The IC_{50} values are the averages (± SEM) of three independent experiments, which are presented in Table 8.

Conclusion

Novel hydrazone ligands and their copper complexes synthesized and characterized were identified as the potent InhA inhibitors. The antitubercular screening of ligands and complexes showed that ligands are less active compared to metal complexes. Among the complexes, **13b** and **13r** have the highest activity (MIC = 0.8 µg/mL) against mycobacteria with no apparent cytotoxicity towards the human lung cancer cell-line (A549). Furthermore, compounds **12r**, **13b** and **13r** have displayed good inhibition activities InhA upto 2.4 µM.

Molecular modeling studies have been carried out for improved understanding of the drug-receptor interaction. Docking simulation studies have shown that these compounds are bound mainly with the substrate binding site of InhA. The 3D QSAR studies of ligands, CoMFA and CoMSIA models have shown high correlative and predictive abilities, based on high bootstrapped r^2 values of 0.88 and 0.74 with a small standard deviation of 0.01%, indicating that a similar relationship exists in all the compounds. The 3D-QSAR models that were developed from the database alignment have shown better correlation with antitubercular activity of the new compounds developed.

Further work to investigate the role of copper ions by determining the lethal dose of the complexes in biological systems and their pharmacological screening is in progress and these results will be reported in our future communication.

Acknowledgments

Authors immensely thank the research support from the Board of Research in Nuclear Sciences (BRNS), Bhabha Atomic Research Centre (BARC), Mumbai (File No. 2013/37B/17/BRNS/0417 dated-14/05/2013). We also thank Dr. V.H. Kulkarni, Principal and Mr. H.V. Dambal, President, SET's College of Pharmacy, Dharwad, India for providing necessary facilities. Authors are also grateful to Mr. Ravindra N. Nadagir for his technical assistance.

References

1. M. Raviglione, B. Marais, K. Floyd, K. Lonnroth, H. Getahun, G.B. Migliori, A.D. Harries, P. Nunn, C. Lienhardt, S. Graham, J. Chakaya, K. Weyer, S. Cole, S.H.E. Kaufmann, A. Zumla, Lancet. 379 (2012) 1902-1913.
2. WHO report. Global Tuberculosis Report, 2012.
3. M.A. Espinal, A. Laszlo, L. Simonsen, F. Boulahbal, S.J. Kim, A. Reniero, S. Hoffner, H.L. Rieder, N. Binkin, C. Dye, R. Williams, M.C. Raviglione, N. Engl. J. Med. 344 (2001) 1294-1303.
4. A. Faustini, A.J. Hall, C.A. Perucci, Thorax. 61 (2006) 158-163.
5. World Health Organization (WHO). 2010.
6. Y. Zhang, B. Heym, B. Allen, D. Young, S. Cole, Nature. 358 (1992) 591-593.
7. K. Johnsson, D.S. King, P.G. Schultz, J. Am. Chem. Soc. 117 (1995) 5009-5010.
8. S.D. Joshi, S.R. Dixit, U.A. More, T.M. Aminabhavi, V.H. Kulkarni, A.K. Gadad, Mini. Rev. Med. Chem. 14 (2014) 678-693.
9. R.J. Heath, J. Li, G.E. Roland, C.O. Rock, J. Biol. Chem. 275 (2000) 4654-4659.
10. R.J. Heath, C.O. Rock, J. Biol. Chem. 270 (1995) 26538-26542.
11. A. Banerjee, E. Dubnau, A. Quemard, V. Balasubramanian, K.S. Um, T. Wilson, D. Collins, G. de-Lisle, W.R. Jacobs Jr, Science 263 (1994) 227-230.
12. A. Quemard, J.C. Sacchettini, A. Dessen, C. Vilcheze, R. Bittma, W.R. Jacobs Jr, J.S. Blanchard, Biochemistry 34 (1995) 8235-8241.
13. H. Lu, P.J. Tonge, Acc. Chem. Res. 41 (2008) 11-20.
14. C. Baldock, J.B. Rafferty, S.E. Sedelnikova, P.J. Baker, A.R. Stuitje, A.R. Slabas, T.R. Hawkes, D.W. Rice, Science. 274 (1996) 2107-2110.
15. H. Kitagawa, K. Kumura, S. Takahata, M. Iida, K. Atsumi, Bioorg. Med. Chem. 15 (2007) 1106-1116.

16. M.A. Seefeld, W.H. Miller, A.N. Kenneth, W.J. Burgess, W.E. DeWolf Jr, P.A. Elkins, M.S. Head, D.R. Jakas, C.A. Janson, P.M. Keller, P.J. Manley, T.D. Moore, D.J. Payne, S. Pearson, B.J. Polizzi, X. Qiu, S.F. Rittenhouse, I.N. Uzinskas, N.G. Wallis, W.F. Huffman, J. Med. Chem. 46 (2003) 1627-1635.
17. L.M. McMurry, M. Oethinger, S.B. Levy, Nature. 394 (1998) 531-532.
18. M. Chhibber, G. Kumar, P. Parasuraman, T.N. Ramya, N. Surolia, A. Surolia, Bioorg. Med. Chem. 14 (2006) 8086-8098.
19. M. Biava, R. Fioravanti, G.C. Porretta, G. Sleiter, A. Ettorre, D. Deidda, G. Lampis, R. Pompei, Med. Chem. Res. 7 (1997) 228-250.
20. D. Deidda, G. Lampis, R. Fioravanti, M. Biava, G.C. Porretta, S. Zanetti, R. Pompei, Antimicrob. Agents. Chemother. 42 (1998) 3035-3037.
21. L.V. Rosa, G. Poce, J.O. Canseco, S. Buroni, M.R. Pasca, M. Biava, R.M. Raju, G.C. Porretta, S. Alfonso, C. Battilocchio, B. Javid, F. Sorrentino, T.R. Loerger, J.C. Sacchettinic, F. Manetti, M. Botta, A.D. Logu, E.J. Rubin, E.D. Rossi, Antimicrob. Agents. Chemother. 56 (2012) 324-331.
22. C. Varela, D. Rittmann, A. Singh, K. Krumbach, K. Bhatt, L. Eggeling, G.S. Besra, A. Bhatt, Chemistry and Biology 19 (2012) 498-506.
23. T.M. Aminabhavi, N.S. Biradar, C.S. Patil, W.E. Rudzinski, Inorg Chem Acta 78 (1983) 107-111.
24. N.S. Biradar, G.V. Karajagi, T.M. Aminabhavi, W.E. Rudzinski, Inorg Chem Acta 74 (1983) 39-41.
25. N.S. Biradar, G.V. Karajagi, T.M. Aminabhavi, W.E. Rudzinski, Inorg Chem Acta 91 (1984) 49-52.
26. A. Robertazzi, A. Magistrato, P.D. Hoog, P. Carloni, J. Reedijk, Inorg. Chem. 46 (2007) 5873-5881.

27. B.C. Bales, M. Pitie, B. Meunier, M.M. Greenberg, J. Am. Chem. Soc. 124 (2002) 9062-9063.

28. M. Nath, P.K. Saini, Dalton. Trans. 40 (2011) 7077-7121.

29. K. Serbest, A. Ozen, Y. Unver, M. Er, I. Degirmencioglu, K. Sancak, J. Mol. Struct. 922 (2009) 1-10.

30. S.B. Bhise, R.J. Dias, S.C. Dhawale, K.K. Mali, Laboratory manual of bio pharmaceutics and pharmacokinetics. Trinity publication house, satara, maharastra, India.

31. U.A. More, S.D. Joshi, T.M. Aminabhavi, V.H. Kulkarni, A.M. Badiger, C. Lherbet, Eur. J. Med. Chem. 94 (2015) 317-339.

32. S.D. Joshi, S.R. Dixit, M.N. Kirankumar, T.M. Aminabhavi, K.V.S.N. Raju, R. Narayan, C. Lherbet, K.S. Yang. Eur. J. Med. Chem. 107 (2016) 133-152.

33. Tripos International, Sybyl-X 2.1.1, Tripos International, St. Louis, MO, USA, 2012.

34. M. Clark, D. Richard, R.D. Cramer III, N.V. Opdenbosch, J. Comput. Chem. 10 (1989) 982-1012.

35. R.D. Cramer III, D.E. Patterson, J.D. Bunce, Prog. Clin. Biol. Res. 291 (1989) 161-165.

36. G.A. Marcoulides, Taylor and Francis, New Jersey, 2009, pp 295-336.

37. G. Thomas, Structure–activity and quantitative structure relationships. In: medicinal chemistry an introduction, 2nd Edn, Wiley, New York, 2007, pp 75-110.

38. M. Nath, P. Arora, Synth. React. Inorg. Met-Org. Chem. 23 (1993) 1523-1546.

39. N.T. Abdel-Ghani, O.E. Sherif, Thermochim. Acta. 156 (1989) 69-83.

40. Y.M. Issa, H.M. Abdel-Fattah, A.A. Soliman, J. Therm. Anal. 42 (1994) 1175-1184.

41. A.M.G. Macdonald, P. Sirichanya, Microchemical Journal 14 (1996) 199-206.

42. J.S. Oliveira, J.H. Pereira, F. Canduri, N.C. Rodrigues, O.N. de Souza, W.F. Azevedo Jr., L.A. Basso, D.S. Santos, J. Mol. Biol. 359 (2006) 646-666.

43. T. Delaine, V. Bernades-Genisson, A. Quémard, P. Constant, B. Meunier, J. Bernadou, Eur. J. Med. Chem. 45 (2010) 4554-4561.

44. B.S. Furniss, A.J. Hannaford, P.W.G. Smith, A.R. Tatchell, Vogel's practical organic chemistry 5th edition, Longman Scientific and Technical, John Wiley & Sons, Inc., New York. pg. 1261.

45. S.D. Joshi, H.M. Vagdevi, V.P. Vaidya, G.S. Gadaginamath, Eur. J. Med. Chem. 43 (2008) 1989-1996.

46. C. Menendez, S. Gau, C. Lherbet, F. Rodriguez, C. Inard, M.P. Rosalia, M. Baltas, Eur. J. Med. Chem. 46 (2011) 5524-5531.

47. C. Menendez, A. Chollet, F. Rodriguez, C. Inard, M.R. Pasca, C. Lherbet, M. Baltas, Eur. J. Med. Chem. 52 (2012) 275-283.

48. A. Chollet, G. Mori, C. Menendez, F. Rodriguez, I. Fabing, M.R. Pasca, J. Madacki, J. Korduláková, P. Constant, A. Quémard, V. Bernardes-Génisson, C. Lherbet, M. Baltas, Eur. J. Med. Chem. 101 (2015) 218-235.

49. C. Maria, S. Lourenco, V. Marcus, N. deSouza, C.P. Alessandra, L.F. Marcelle de, B. Rasnisb, Goncalves, C.M.N. Thais, A.P. Monica, ARKIVOC 15 (2007) 181-191.

50. T. Mosmann. J. Immunol. Methods. 65 (1983) 55-63.

51. L.L. Gundersen, J. Nissen-Meyer, B. Spilsberg, J. Med. Chem. 45 (2002) 1383-1386.

Scheme 1. Synthetic route of a series of 3-oxo-*N*-substituted phenylpentamides or 2-oxo-*N*-substituted phenylpropamides

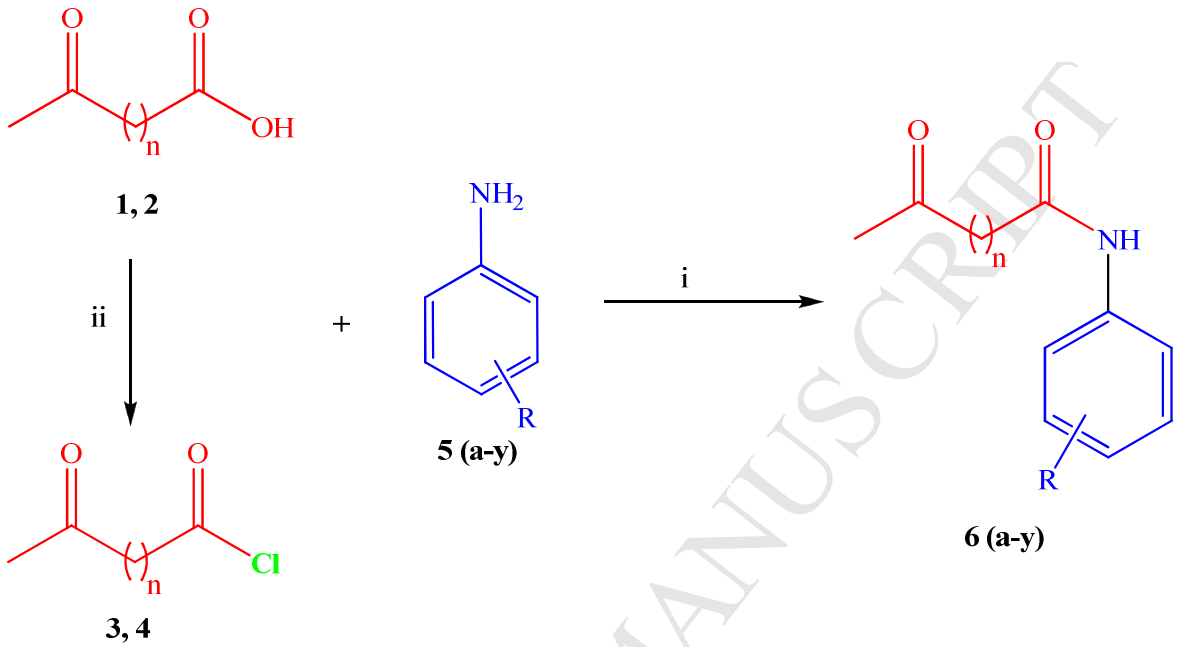

n = 0, 2

Reagents and reaction conditions: i) HBTU, DIEA, DMF, Starring, 8-10 h; **ii)** Thionyl chloride, diethyl ether or chloroform, heated up to 70ºC.

Scheme 2. Synthesis of pyrrole and dimethyl pyrrole hydrazides

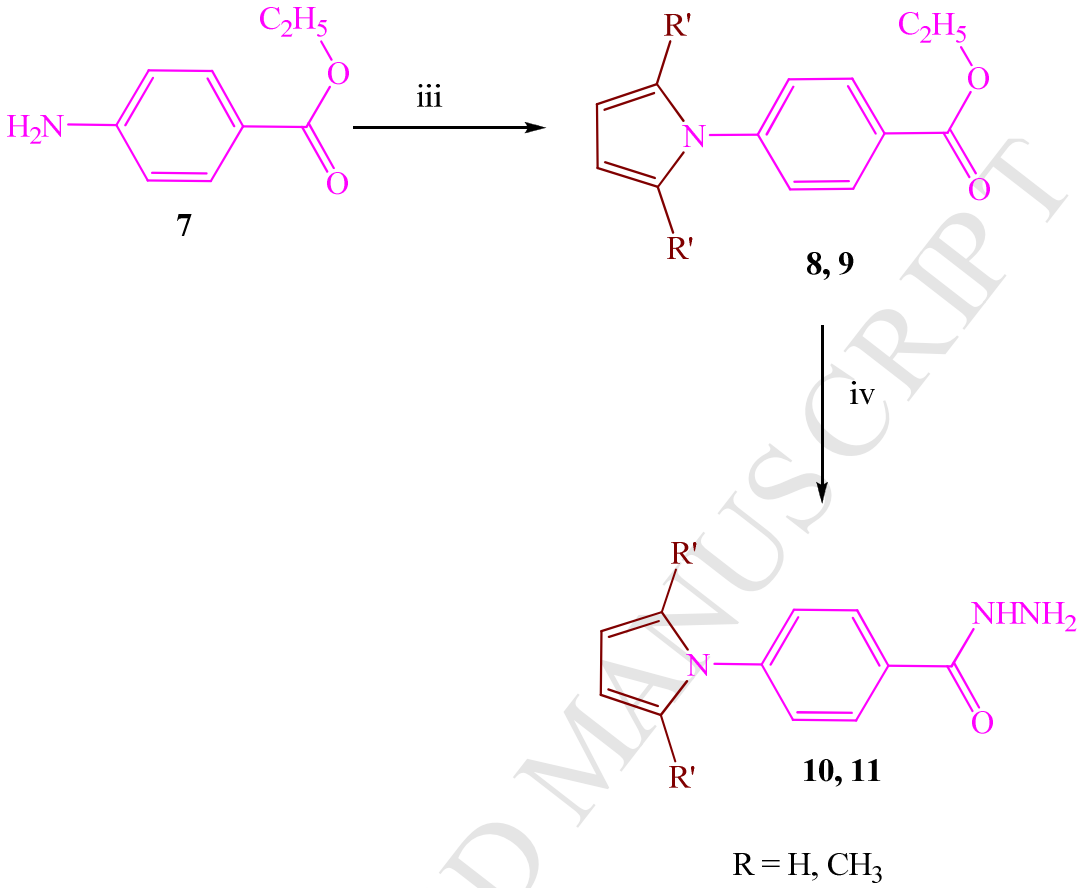

Reagents and reaction conditions: iii) 2,5-dimethoxytetrahydrofuran/2,5-hexanedione, acetic acid, reflux, 45 min; **iv)** $NH_2NH_2.H_2O$, ethanol, reflux, 3 h.

Scheme 3. Synthetic route of a novel series of pyrrolyl hydrazone derivatives.

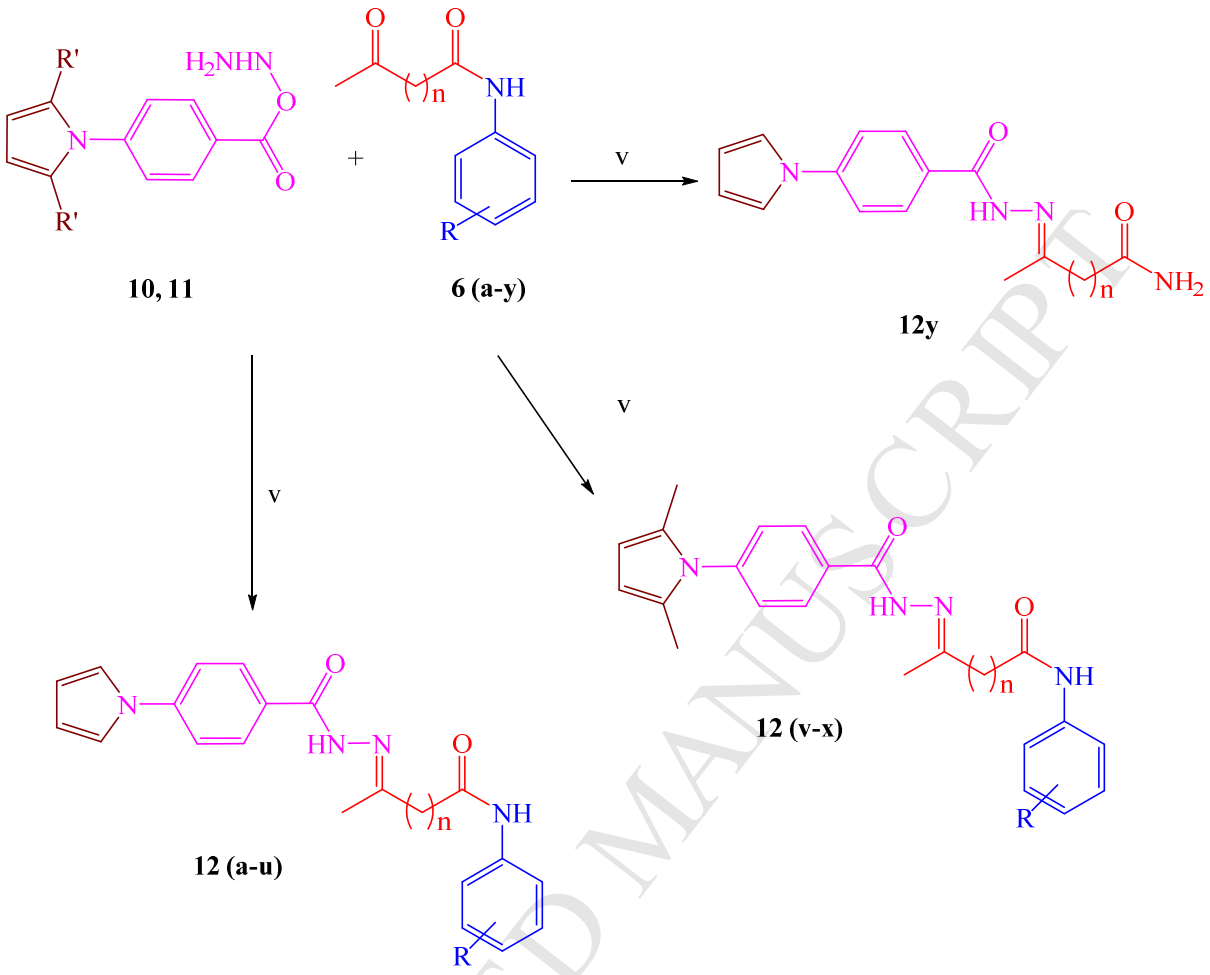

n = 0, R'= -H

	R
12a	3-Br
12b	4-Br
12c	2,6-Cl
12d	3,5-Cl
12e	4-OCH_3
12f	3-OCH_3
12g	3-F
12h	4-F
12i	2-F
12j	3,5-Br

n = 2, R'= -H

	R
12k	4-Br
12l	3-Br
12m	2-Cl
12n	3-Cl
12o	4-Cl
12p	3,5-Cl
12q	2-OCH_3
12r	4-F
12s	3-F
12t	2-F
12u	-H

n = 0, R'= -CH_3

	R
12v	4-Br
12w	2,6-Cl
12x	4-OCH_3

Reagents and reaction conditions: v) Ethanol, reflux, 72-78 h.

Scheme 4. Synthetic route of a novel series of biologically active metal complexes.

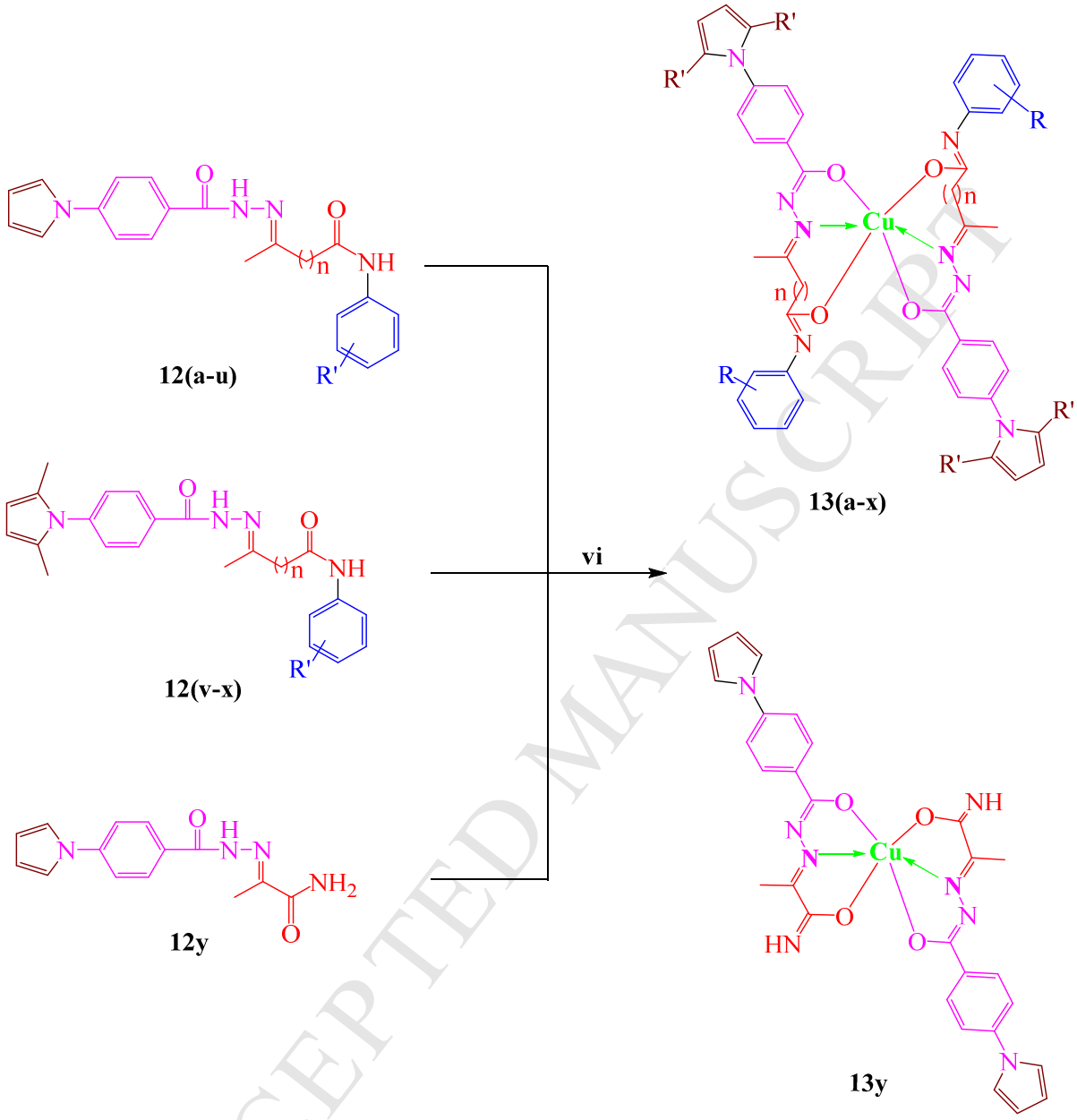

Reagents and reaction conditions: vi) Copper acetate, ethanol, reflux, 58-60 h.

Table 1: List of the derivatives with their substitution pattern, biological activity.

Comp.	R	R'	MIC values (µg/mL) *M. tuberculosis* H37Rv	Comp.	R	R'	MIC values (µg/mL) *M. tuberculosis* H37Rv
12a	-H	3-Br	12.5	**13a**	-H	3-Br	6.25
12b	-H	4-Br	3.12	**13b**	-H	4-Br	0.8
12c	-H	2,6-diCl	25	**13c**	-H	2,6-diCl	12.5
12d	-H	3,5-diCl	12.5	**13d**	-H	3,5-diCl	6.25
12e	-H	4-OCH_3	50	**13e**	-H	4-OCH_3	25
12f	-H	3-OCH_3	50	**13f**	-H	3-OCH_3	25
12g	-H	3-F	12.5	**13g**	-H	3-F	6.25
12h	-H	4-F	6.25	**13h**	-H	4-F	1.6
12i	-H	2-F	25	**13i**	-H	2-F	12.5
12j	-H	3,5-diBr	25	**13j**	-H	3,5-diBr	12.5
12k	-H	4-Br	6.25	**13k**	-H	4-Br	3.12
12l	-H	3-Br	25	**13l**	-H	3-Br	12.5
12m	-H	2-Cl	25	**13m**	-H	2-Cl	50
12n	-H	3-Cl	12.5	**13n**	-H	3-Cl	6.25
12o	-H	4-Cl	3.12	**13o**	-H	4-Cl	1.6
12p	-H	3,5-diCl	25	**13p**	-H	3,5-diCl	25
12q	-H	2-OCH_3	100	**13q**	-H	2-OCH_3	100
12r	-H	4-F	3.12	**13r**	-H	4-F	0.8
12s	-H	3-F	12.5	**13s**	-H	3-F	6.25
12t	-H	2-F	25	**13t**	-H	2-F	12.5
12u	-H	-H	50	**13u**	-H	-H	25
12v	-CH_3	4-Br	12.5	**13v**	-CH_3	4-Br	6.25
12w	-CH_3	2,6-diCl	100	**13w**	-CH_3	2,6-diCl	50
12x	-CH_3	4-OCH_3	100	**13x**	-CH_3	4-OCH_3	50
12y	--	--	50	**13y**	--	--	25
		Ethambutol			--	--	0.5
		Rifampicin			--	--	0.4

Table 2. Statistical parameters of CoMFA and CoMSIA models by the PLS analysis

Method	Parameters	CoMFA		CoMSIA	
Cross validation	Optimal components	2		2	
	r^2_{loo}	0.86		0.69	
	r^2_{pred}	0.83		0.64	
	r^2_{bs}	0.88		0.74	
	SD_{bs}	0.01		0.04	
	q^2	0.75		0.62	
Non-cross validation	r^2	0.88		0.74	
	SEE	0.12		0.17	
	F	97.12		42.00	
PLS parameters		Norm coefficient	Fraction	Norm coefficient	Fraction
	Steric	0.72	0.26	0.15	0.18
	Electronic	0.73	0.27	0.15	0.23
	H-bond donor	-	-	0.01	0.11
	H-bond acceptor	-	-	0.16	0.21

Table 3. Thermoanalytical data

Comp.	Loss of solvent % found (calc.)	Decomposition stage °C	Metallic residue %found (calc.)
13a	3.51 (3.63)	250.27-280.34	37.96 (38.59)
13b	3.54 (3.32)	248.76-285.51	37.79 (38.59)
13c	3.65 (3.32)	268.57-310.42	35.53 (35.91)
13d	3.48 (3.32)	268.61-310.46	35.67 (35.91)
13e	3.57 (3.32)	269.78-297.52	38.86 (39.26)
13f	3.52 (3.32)	269.68-297.50	38.82 (39.26)
13g	3.61 (3.32)	274.86-314.72	44.06 (44.38)
13h	3.54 (3.32)	274.81-314.64	44.13 (44.38)
13i	3.65 (3.32)	267.57-306.34	37.57 (37.78)
13j	3.59 (3.32)	241.65-285.27	29.67 (30.05)
13k	3.62 (3.32)	239.48-271.42	36.84 (37.48)
13l	3.56 (3.32)	239.60-271.48	36.81 (37.48)
13m	3.53 (3.32)	274.27-300.24	26.43 (26.68)
13n	3.49 (3.32)	274.35-300.29	25.76 (26.68)
13o	3.63 (3.32)	274.27-300.41	25.71 (26.68)
13p	3.67 (3.32)	258.91-290.80	32.86 (33.79)
13q	3.62 (3.32)	241.51-268.81	36.15 (36.74)
13r	3.59 (3.32)	267.64-306.43	37.53 (37.78)
13s	3.64 (3.32)	267.61-306.40	37.50 (37.78)
13t	3.60 (3.32)	274.77-314.68	44.16 (44.38)
13u	3.63 (3.32)	270.68-292.71	39.02 (39.55)
13v	3.65 (3.32)	286.58-307.80	36.37 (35.30)
13w	3.64 (3.32)	258.98-290.86	32.98 (33.79)
13x	3.50 (3.32)	241.47-268.78	35.87 (36.74)
13y	3.68 (3.63)	239.61-284.54	66.07 (66.10)

Table 4. Interaction energy and different scores of the ligands docked on the mutant protein 2AQI.

Comp.	Total score	Crash	Polar	D_score	PMF_score	G_score	Chem score
12r (template)	8.01	-2.14	1.01	-456.43	-11.58	-216.65	-44.72
12b	7.96	-1.92	0.68	-381.58	13.77	-161.12	-41.39
12o	7.58	-0.70	0.08	-381.41	13.73	-161.14	-33.01
12k	7.13	-1.33	2.21	-378.86	-32.26	-176.15	-37.75
12v	6.89	-2.22	1.00	-323.24	29.58	-154.52	-33.87
12y	6.74	-1.50	1.74	-351.79	-12.23	-145.03	-25.20
12s	6.54	-2.70	2.19	-550.57	17.93	-265.26	-45.209
12n	6.38	-1.39	2.58	-432.98	35.46	-206.99	-39.99
12h	6.13	-1.32	1.46	-375.03	-29.46	-180.72	-37.47
12i	5.83	-2.26	1.56	-415.75	7.77	-239.41	-39.07
12l	5.74	-1.81	1.42	-343.25	2.92	-244.32	-38.15
12d	5.63	-1.25	1.55	-338.63	23.27	-160.61	-34.21
12g	5.31	-0.85	0.04	-439.69	-26.14	-148.95	-28.57
12u	5.04	-1.57	2.04	-404.66	-36.04	-183.88	-37.87
12e	4.87	-1.07	1.87	-338.71	23.04	-160.04	-34.74
12f	4.70	-1.00	1.51	-338.30	23.72	-160.81	-34.53
12a	4.52	0.55	2.05	-281.81	28.15	-166.37	-36.50
12w	4.47	0.14	2.81	-281.14	28.72	-166.81	-36.73
12m	4.31	-0.93	0.05	-381.58	13.77	-161.12	-33.54
12p	4.08	-1.07	2.72	-338.81	23.85	-160.46	-34.51
12c	4.01	-1.22	2.10	-320.64	1.15	-168.32	-37.19
12x	3.97	0.48	1.07	-343.57	13.71	-157.46	-33.00
12q	3.81	-1.40	1.00	-343.70	13.81	-157.75	-33.81
12t	3.81	-1.21	1.85	-343.94	13.41	-157.74	-33.09
12j	3.36	-1.22	2.00	-327.79	-12.50	-163.72	-34.13

Table 5. Interaction energy and different scores of the metal complexes docked on the mutant protein 2AQI.

Comp.	Total score	Crash	Polar	D_score	PMF_score	G_score	Chem score
13r	12.71	-2.97	1.05	1016.686	22.902	-445.171	-36.106
13b	11.96	-1.92	0.00	1234.002	29.025	-399.760	-31.438
13o	9.55	-2.01	0.00	1222.369	28.697	-406.182	-34.580
13a	9.38	-3.86	0.00	1073.870	0.159	-432.631	-43.421
13k	9.29	-2.97	0.65	1136.427	23.801	-411.775	-32.664
13s	9.11	-3.17	2.31	980.242	16.314	-340.503	-28.615
13n	8.41	-1.65	3.26	1085.624	2.498	-331.482	-30.169
13y	7.53	-4.34	0.75	1003.289	40.102	-425.806	-40.613
13w	7.37	-1.20	0.75	912.275	-6.007	-338.476	-33.672
13t	7.26	-0.88	2.38	1059.131	-20.463	-295.112	-32.768
13f	6.54	-4.98	0.11	1205.227	27.952	-436.834	-40.176
13v	6.52	-2.50	2.73	1410.152	61.589	-336.046	-24.232
13l	6.44	-3.32	2.29	1264.061	-2.120	-368.003	-32.404
13i	6.25	-2.38	2.95	1350.163	24.482	-295.556	-28.386
13q	6.10	-3.97	0.64	817.306	40.859	-326.603	-35.375
13g	5.78	-3.47	0.91	1464.845	64.712	-382.567	-32.032
13u	5.73	-5.41	0.00	869.125	43.538	-423.565	-34.371
13p	5.71	-8.19	2.22	1055.689	40.124	-496.237	-40.286
13d	5.66	-2.35	2.31	1096.844	-28.357	-274.380	-34.222
13m	5.52	-3.57	1.05	1146.235	61.437	-352.218	-31.282
13h	5.46	-2.62	0.00	1428.677	39.853	-372.729	-33.375
13j	5.43	-3.33	0.00	1394.593	17.413	-411.612	-37.313
13x	5.39	-5.55	0.00	1298.987	46.321	-460.721	-36.827
13e	5.39	-2.03	0.00	1099.698	40.259	-307.836	-26.329
13c	5.02	-3.56	0.10	1207.928	26.471	-437.167	-32.815

Table 6. Actual (Act.) and predicted (Pred.) pMIC values and residuals (Δ) of the database aligned training set and test set molecules.

Comp.	MIC	Act. pMIC	CoMFA		CoMSIA	
			Pred. pMIC	Δ	Pred. pMIC	Δ
Training set						
12v	6.25	5.20	4.88	0.32	4.86	0.34
12y	50.00	4.30	4.37	-0.07	4.42	-0.12
12b	3.12	5.50	5.12	0.38	5.10	0.40
12k	6.25	5.20	5.29	-0.09	5.29	-0.09
12m	25.00	4.60	4.69	-0.09	4.68	-0.08
12r	25.00	4.60	4.85	-0.25	4.89	-0.29
12o	3.12	5.50	5.30	0.2	5.30	0.20
12w	100.00	4.00	4.04	-0.04	4.02	-0.02
12c	25.00	4.60	4.42	0.18	4.39	0.21
12d	12.50	4.90	4.74	0.16	4.75	0.15
12e	50.00	4.30	4.37	-0.07	4.42	-0.12
12f	50.00	4.30	4.22	0.08	4.18	0.12
12x	25.00	4.60	4.69	-0.09	4.68	-0.08
12g	25.00	4.58	4.57	0.01	4.58	0.00
12r	3.12	5.50	5.30	0.2	5.30	0.20
12s	25.00	4.60	4.78	-0.18	4.80	-0.20
12i	50.00	4.30	4.18	0.12	4.20	0.10
12t	25.00	4.60	4.45	0.15	4.453	0.14
12j	12.50	4.90	5.03	-0.13	5.01	-0.11
Test set						
12a	12.50	4.90	4.89	0.05	4.92	0.01
12l	12.50	4.90	4.85	0.21	4.89	0.24
12p	25.00	4.60	4.39	0.05	4.36	0.03
12q	100.00	4.00	3.95	-0.13	3.97	-0.11
12h	6.25	5.20	5.33	0.05	5.31	0.05
12u	50.00	4.30	4.25	0.38	4.25	0.34

Table 7. Enzyme inhibition values. Results are expressed as % InhA inhibition.

Compound	% Inhibition at 50 µM InhA
12o	29
12h	13
13k	24
12b	35
12k	2
13h	19
13o	32
13r	100 (IC_{50} = 2.42 ± 0.21 µM)
13b	100 (IC_{50} = 2.38 ± 0.02 µM)
12r	91 (IC_{50} = 7.69 ± 0.96 µM)
Triclosan	> 99

Table 8. Cytotoxicity activity against human lung cancer cell line A549.

Compound	IC_{50} µM
12b	441±0.1
12o	406±0.3
12r	438±0.2
13b	281±0.2
13k	252±0.1
13o	289±0.3
13r	305±0.2
Isoniazid	>450
Cisplatin	1.29

IC_{50} - is half maximal inhibitory concentration- it is the half maximal (50%) inhibitory concentration (IC) of a substance (50% IC, or IC_{50})

Fig. 1. Design and development of potent enoyl ACP-reductase inhibitor by the incorporation of the traditional fragment based drug design and modern drug design tools.

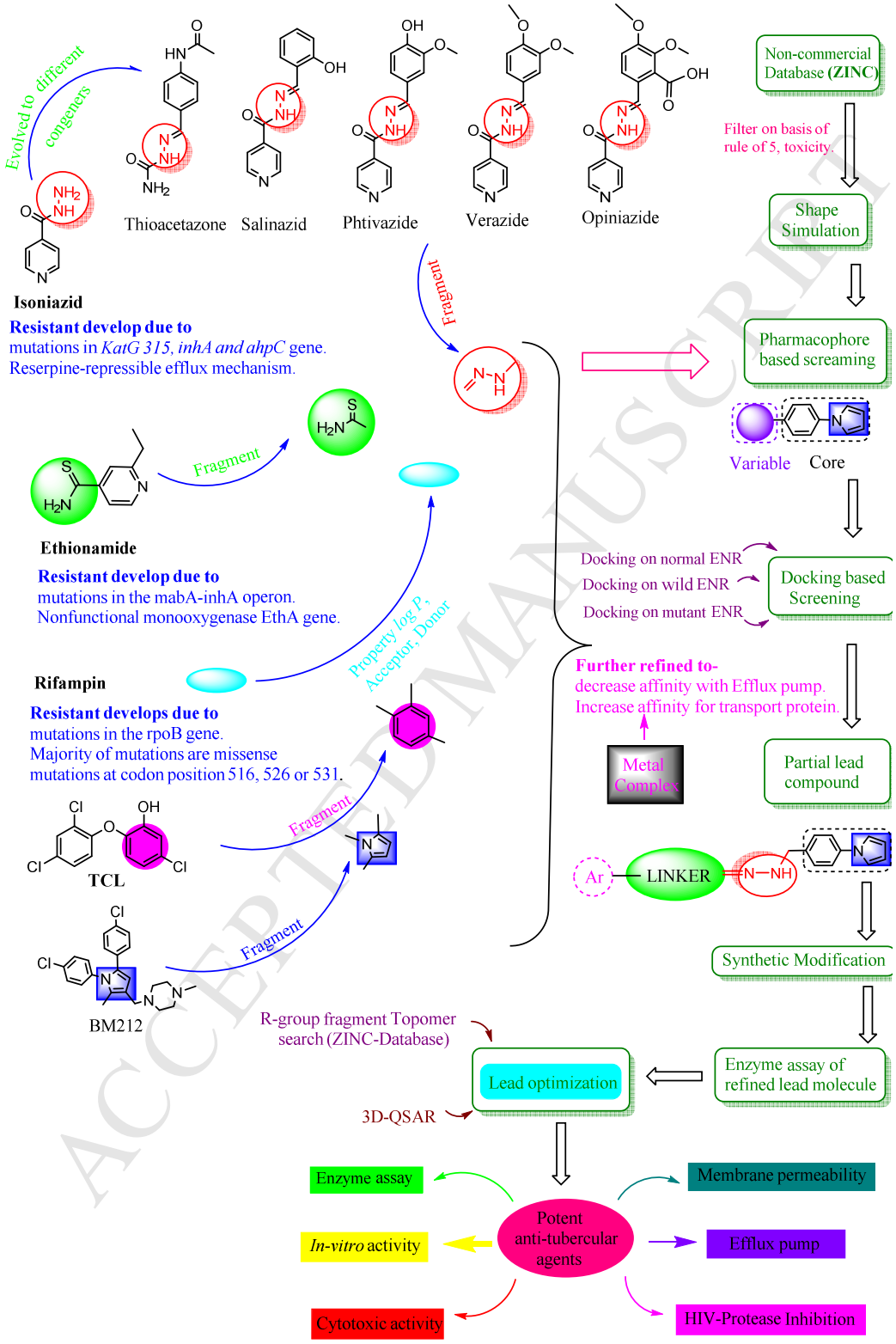

Fig. 2 (A & B). Interaction pattern of modified lead molecule **(12r)** shows the new pattern of interaction with mutant ENR protein (2AQI).

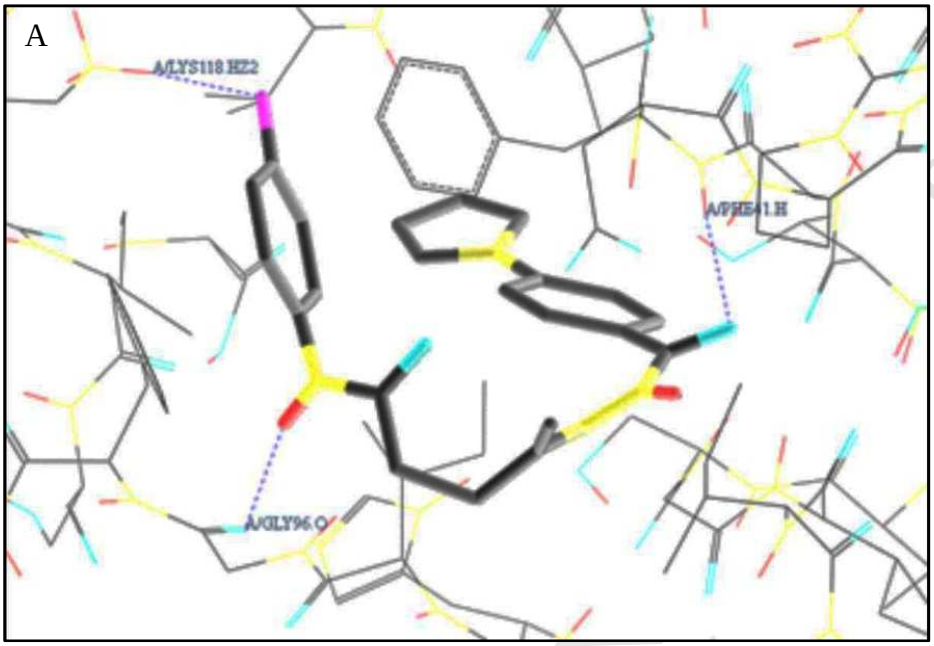

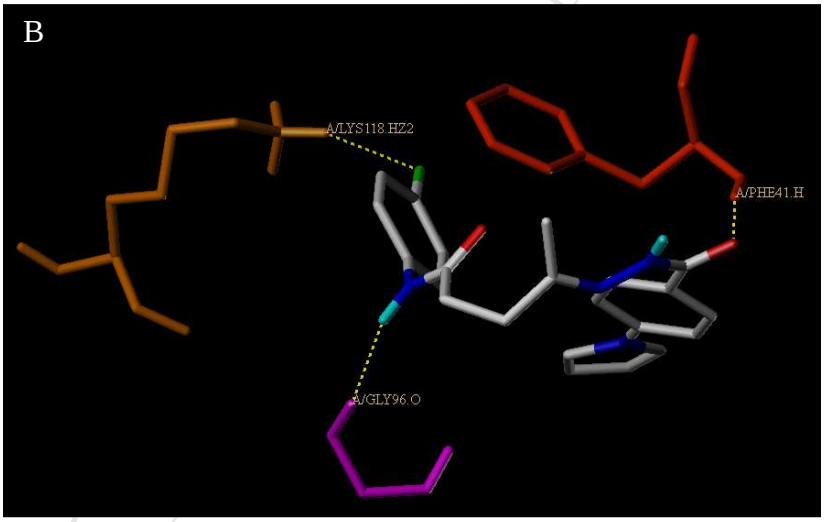

Fig. 3 (A & B). Spatial orientation and pattern of interaction of metal complex **(13b)** with mutant ENR enzyme (2AQI).

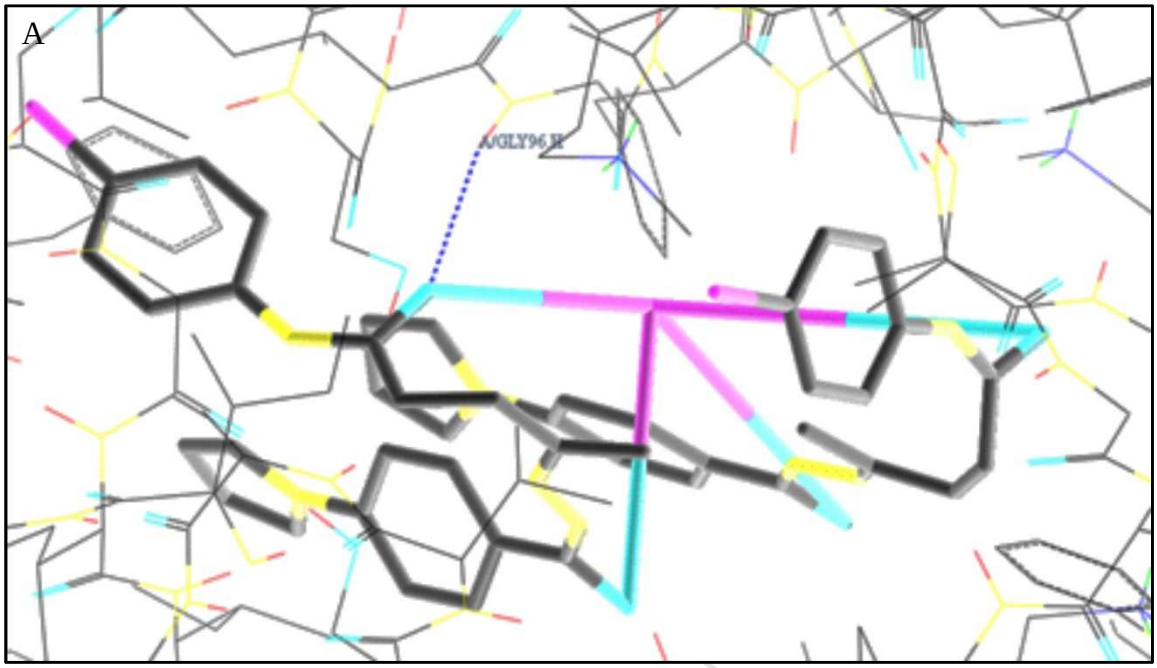

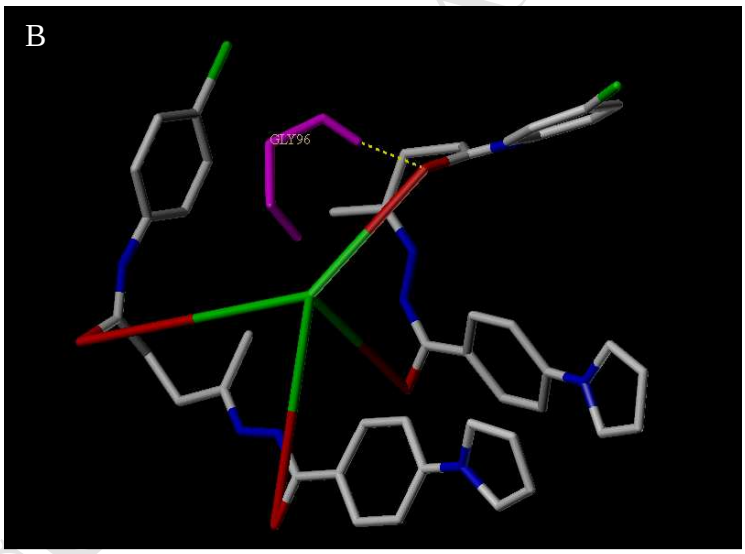

Fig. 4. CoMFA contour map of final analysis with 2Å grid spacing **(12b)**. (A) Steric contour map. Orange contour refers to sterically favored regions; blue contour indicates sterically disfavored areas. (B) Electrostatic contour map. Yellow contours refer to the region where positively charged substituents are favored; skyblue contours indicate the regions where negatively charged substituents are favored.

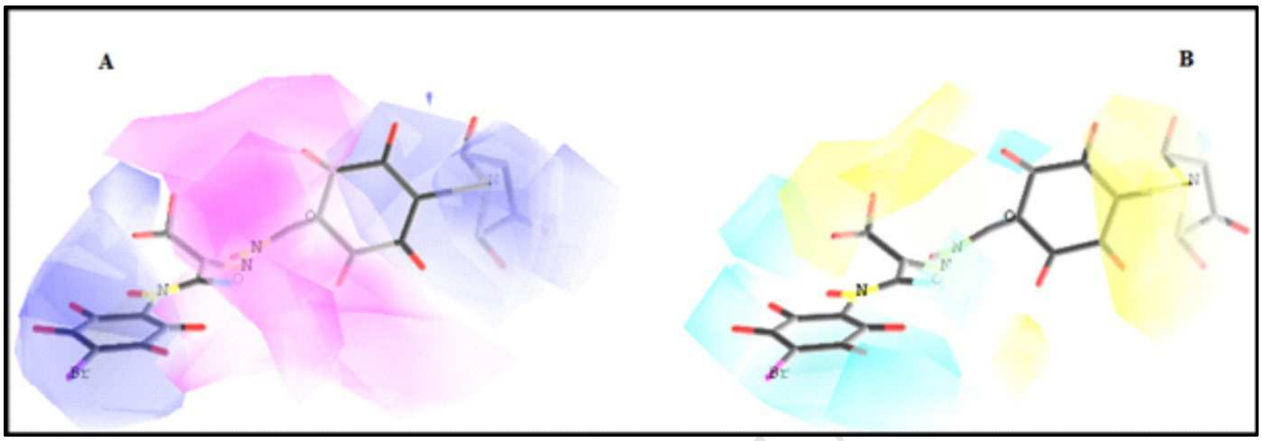

Fig. 5. Contour maps of final CoMSIA analysis with 2Å grid spacing **(12b)**. (A) Steric contour maps, orange contours refer to sterically favored region; blue contours indicate disfavored areas. (B) Yellow contours refer to regions where negatively charged substituents are disfavored; cyan contours indicate the regions where negatively charged substituents are favored. (C) H-bond acceptor contour map, green contours encompass regions where hydrogen-bond donors on the receptor are expected. Cyan contours refer to areas where hydrogen-bond on the receptor decreases the affinity. (D) H-bond donor contour map, pink contours encompass regions where hydrogen-bond donors bulk desirable. Yellow contours refer to areas where hydrogen-bond donor bulk undesirable. (E) Hydrophobic contour maps, grey contours refer to regions where hydrophilic substituents are favored; purple contours indicate the regions where hydrophobic substituents favored.

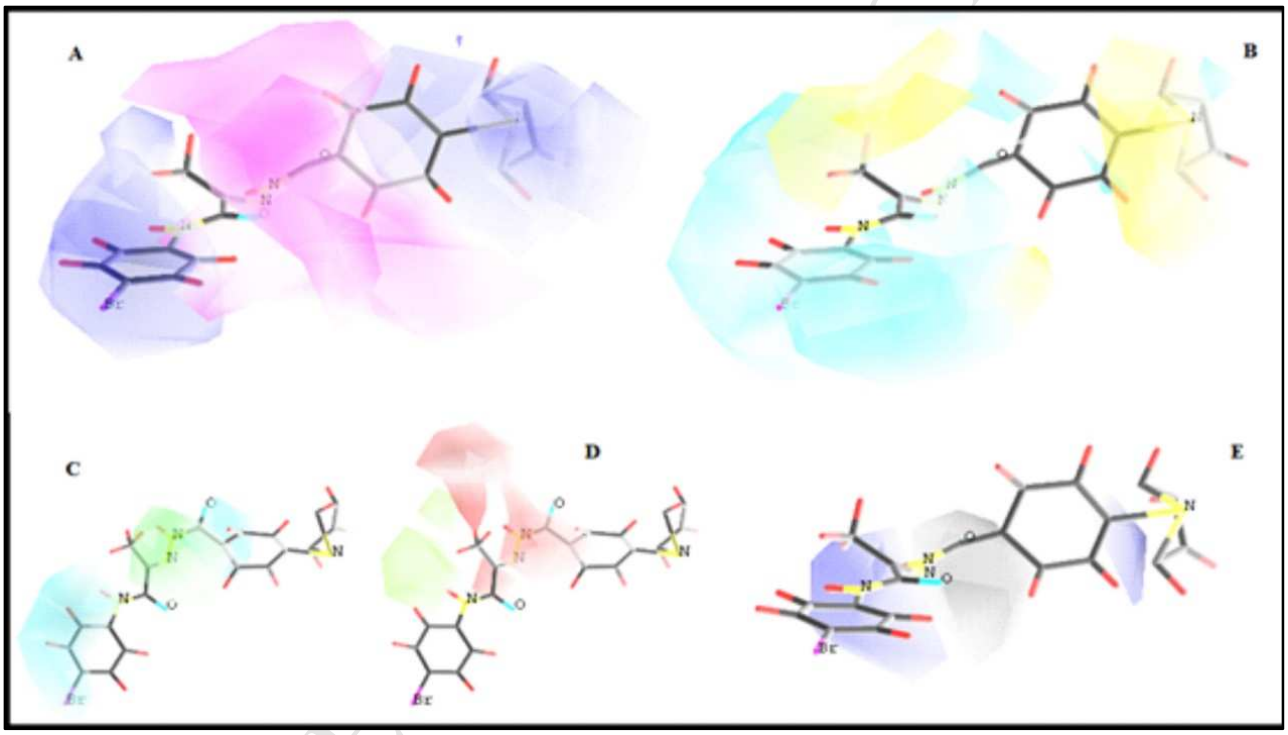

Fig. 6. Structure-activity relationship.

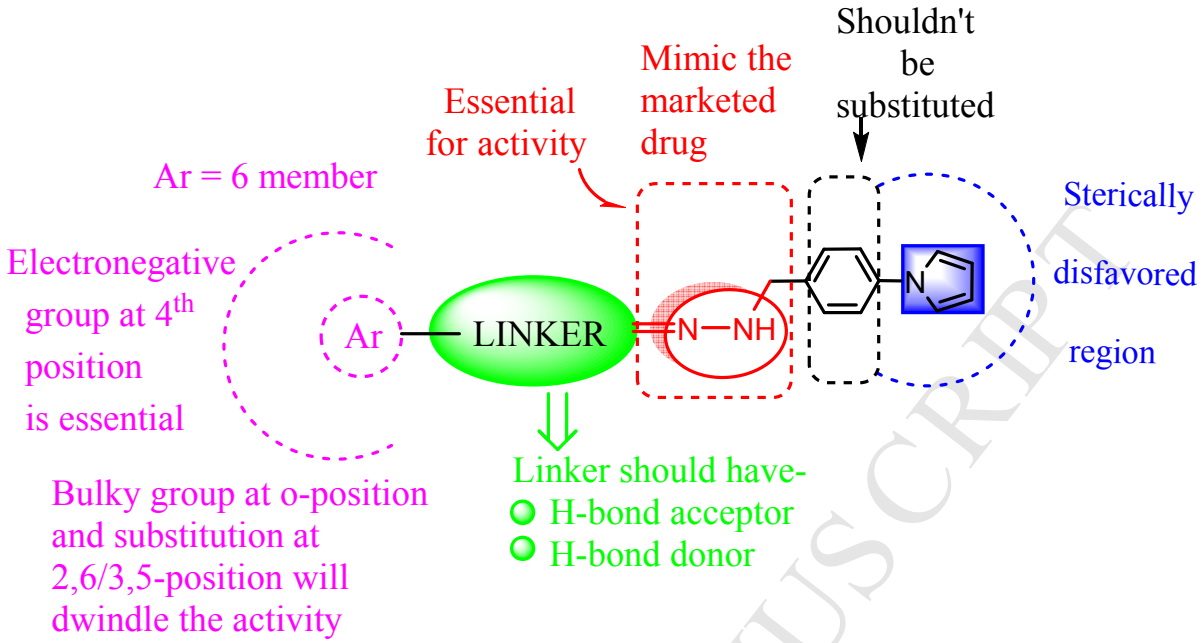

Research Highlights

- Inhibitors of mycobacterial Enoyl ACP reductase were designed using in *silico* approach.
- Synthesis of a range of these pyrrolyl Schiff bases, pyrrolyl Cu-complexes is described.
- Surflex docking studies were carried out to understand the binding affinity of the compounds
- Inhibitors were active against *Mycobacterium tuberculosis, and InhA.*